



# Accelerating axonal growth promotes motor recovery after peripheral nerve injury in mice

Chi Him Eddie Ma,<sup>1</sup> Takao Omura,<sup>1</sup> Enrique J. Cobos,<sup>1</sup> Alban Latrémolière,<sup>1</sup> Nader Ghasemlou,<sup>1</sup> Gary J. Brenner,<sup>2</sup> Ed van Veen,<sup>3</sup> Lee Barrett,<sup>1</sup> Tomokazu Sawada,<sup>4</sup> Fuying Gao,<sup>5</sup> Giovanni Coppola,<sup>5</sup> Frank Gertler,<sup>3</sup> Michael Costigan,<sup>1</sup> Dan Geschwind,<sup>5,6</sup> and Clifford J. Woolf<sup>1</sup>

<sup>1</sup>Program in Neurobiology and F.M. Kirby Neurobiology Center, Children's Hospital Boston, and Department of Neurobiology, Harvard Medical School, Boston, Massachusetts, USA. <sup>2</sup>Department of Anesthesia and Critical Care, Massachusetts General Hospital, and Harvard Medical School, Boston, Massachusetts, USA.

<sup>3</sup>Koch Institute for Integrative Cancer Research, Massachusetts Institute of Technology, Cambridge, Massachusetts, USA.

<sup>4</sup>Department of Orthopaedic Surgery, Hamamatsu University School of Medicine, Hamamatsu, Shizuoka, Japan. <sup>5</sup>Program in Neurogenetics, Department of Neurology, David Geffen School of Medicine, and <sup>6</sup>Department of Human Genetics, UCLA, Los Angeles, California, USA.

**Although peripheral nerves can regenerate after injury, proximal nerve injury in humans results in minimal restoration of motor function. One possible explanation for this is that injury-induced axonal growth is too slow. Heat shock protein 27 (Hsp27) is a regeneration-associated protein that accelerates axonal growth in vitro. Here, we have shown that it can also do this in mice after peripheral nerve injury. While rapid motor and sensory recovery occurred in mice after a sciatic nerve crush injury, there was little return of motor function after sciatic nerve transection, because of the delay in motor axons reaching their target. This was not due to a failure of axonal growth, because injured motor axons eventually fully re-extended into muscles and sensory function returned; rather, it resulted from a lack of motor end plate reinnervation. Tg mice expressing high levels of Hsp27 demonstrated enhanced restoration of motor function after nerve transection/resuture by enabling motor synapse reinnervation, but only within 5 weeks of injury. In humans with peripheral nerve injuries, shorter wait times to decompression surgery led to improved functional recovery, and, while a return of sensation occurred in all patients, motor recovery was limited. Thus, absence of motor recovery after nerve damage may result from a failure of synapse reformation after prolonged denervation rather than a failure of axonal growth.**

## Introduction

The molecular machinery necessary for axon formation and elongation is present during neural development but absent in the adult nervous system (1–3). However, injury to axons in the peripheral but not the central nervous system can reactivate intrinsic growth programs to enable nerve regeneration, and functional recovery can be achieved, provided injured axons are aligned with their former pathways and close to their targets (4). However, proximal nerve lesions, and even more so those that involve a complete transection of the nerve, generally have a poor outcome with, in particular, minimal clinically meaningful motor recovery (5–7). One proposed explanation for this is that the injury-induced increase in intrinsic axonal growth is too slow; as a consequence, by the time axons reach distal denervated nerves, the substrate for growth may no longer be permissive (8), and functional restoration does not occur because axons never reach their targets (9).

One way to accelerate growth in peripheral axons is a preconditioning nerve injury, which primes sensory neurons into an active growth state as a result of the increased expression of regeneration-associated genes (10, 11). Preinjury of the peripheral axons of dorsal root ganglion (DRG) neurons, for example, increases neurite formation and elongation in vitro as well as the rate of sensory axon regeneration in peripheral nerves (12, 13). Surprisingly, of the many hundreds of genes induced in sensory and motor neurons by

axonal injury, only a few candidate regeneration-associated genes have been identified that increase neurite growth, *Gap43*, *Cap23*, *Tubb2a*, *Sprr1a*, *Fn14*, *Ndel1*, and *Trpc4*, as well as several regeneration-promoting transcription factors, *Atf3*, *c-Jun*, *Stat3*, and *Sox11* (11). Although these proteins individually increase axonal growth, none thus far have been shown to produce functional recovery (Supplemental Table 1; supplemental material available online with this article; doi:10.1172/JCI58675DS1).

The small heat shock protein 27 (Hsp27, official gene symbol *Hspb1*) was one of the first injury-induced genes to be identified in DRG neurons by a differential gene expression strategy (14) and is directly regulated by *Atf3* (13), which binds to its promoter (15). Hsp27 is induced in the soma and axons of sensory and motor neurons after nerve injury (14), and its expression in these neurons prevents apoptosis (16). Missense mutations of *Hspb1* are, in addition, linked to sensory and motor neuropathies in several variants of Charcot-Marie-Tooth disease (17). Expression of Hsp27 in cultured adult DRG neurons enhances neurite growth (18), making it a contributor to axonal growth, possibly as a result of its action in promoting actin polymerization (19, 20), a key component of axonal elongation (21). Hsp27 regulates actin polymerization in a phosphorylation-dependent manner. Dephosphorylated Hsp27 inhibits actin polymerization by functioning both as an F-actin filament capping protein (20) and as an actin monomer sequestering protein (19). In contrast, phospho-Hsp27 stabilizes F-actin (20, 22) to facilitate actin monomer addition to growing filaments, promoting filament elongation (18, 19). Hsp27 and phospho-Hsp27 colocalize with F-actin in lamellipodia and regulate actin dynamics and cytoskeletal remodeling through p38 MAP kinase (20, 22), contributing to cell motility and migration (23). Axonal growth cones use F-actin-based cylindrical protrusions, filopodia, to dynamically

**Authorship note:** Takao Omura, Enrique J. Cobos, Alban Latrémolière, and Nader Ghasemlou contributed equally to this work.

**Conflict of interest:** Clifford J. Woolf owns stock in Ferrumax Pharmaceuticals and received income from Endo Pharmaceuticals and grant support from GSK and Endo Pharmaceuticals.

**Citation for this article:** *J Clin Invest*. 2011;121(11):4332–4347. doi:10.1172/JCI58675.

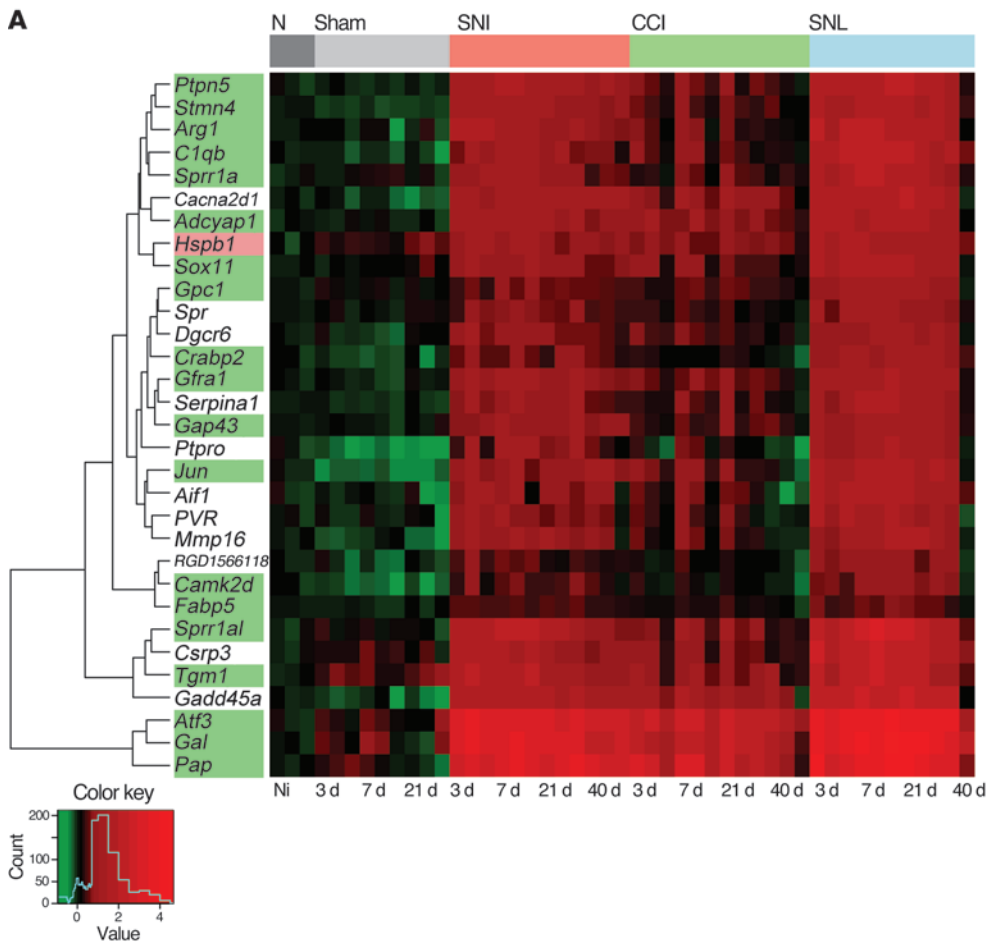
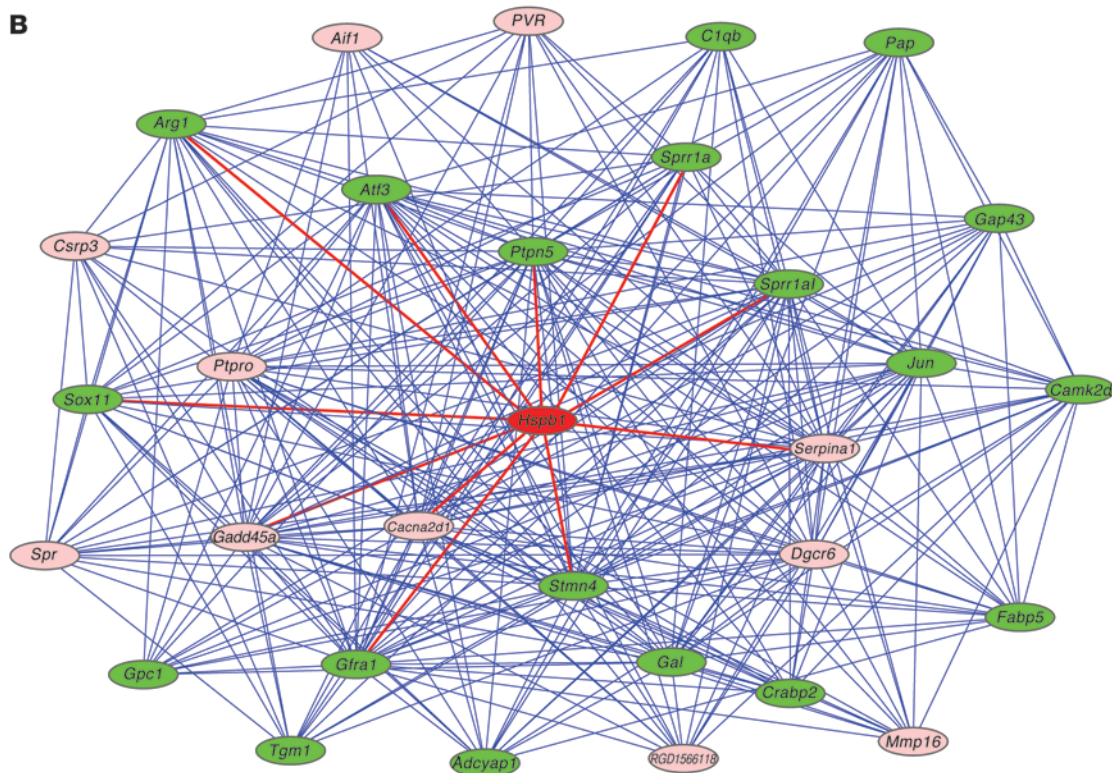


**Figure 1** WGCNA and nearest neighbor analysis (NNA). After building a WGCNA network on a microarray data set using multiple models of DRG injury, *Hspb1* was used as a seed, and the 30 closest neighbors were identified using TO as a measure of connection strength. (A) Heat map depicting fold changes of the top 30 *Hspb1* neighbors in several experimental models of DRG injury (demarcated by the color bar at the top), compared with the average expression in naive (N) samples (dark gray); spared nerve injury (SNI) (red), chronic nerve constriction (green), and spinal nerve ligation (SNL) (blue). Sham lesions are identified in light gray. Genes are clustered by similarity, with upregulated genes in red, and downregulated genes in green. Changes are expressed in log<sub>2</sub> scale. CCI, chronic constriction injury. (B) Visualization of the top 30 nearest neighbors to *Hspb1*. Two connected genes have high TO and therefore share neighbors. Green gene symbols are those known to be involved in regeneration. Top connections of *Hspb1* are depicted in red.





explore, sample, and respond to environmental cues (24). The formation and dynamics of growth cone filopodia are tightly regulated by actin monomer addition at the filopodial tips, the first structures to encounter and respond to environmental information (24).

Because of its induction by peripheral nerve lesions (14), regulation by ATF3 that increases intrinsic growth (13), enhancing effect on neurite growth *in vitro* (18), localization in growth cones (18), and interactions with actin (20, 22), we decided to investigate whether Hsp27 can enhance nerve regeneration and promote functional recovery.

## Results

**Screening for *Hspb1*-associated genes.** To explore the possible role of Hsp27 in regeneration within the context of the whole genome transcriptional response to injury, we performed an unbiased network analysis. Weighted gene coexpression network analysis (WGCNA) allows groups of tightly coexpressed genes to be identified across experimental conditions, effectively uncovering a structure in the transcriptome often not evident after conventional differential expression analysis (25) that can reveal transcriptional modules of functional relevance (25). One application of WGCNA is the network neighborhood analysis (NNA) (19), in which one or more genes are used as a seed, and the network comprising the closest neighbors (i.e., genes with the highest topological overlap (TO) with the seed; see Methods) is built through an iterative process. We applied WGCNA/NNA to a large-scale triplicate microarray DRG data set made up of naive samples and 3 peripheral nerve injury paradigms from 3 to 40 days after injury (ref. 26 and Figure 1A).

We used *Hspb1* as a seed and recursively added the top 30 nearest neighbors following network production (Figure 1B). Sixty-three percent of the closest neighbors identified by this unbiased method were genes directly or indirectly involved in or annotated for regeneration and growth cone dynamics, including *Arg1*, *Atf3*, *C1qb*, *Gal*, *Gap43*, *Gfra1*, *Jun*, *Sox11*, *Sprr1a*, and *Stmn4* (Figure 1 and Supplemental Table 2). Furthermore, several antiapoptotic genes are also represented (23%), but relatively few of the many genes related to pain and dysregulated after DRG peripheral injury (27) are included in the list (10%) (Supplemental Table 2). This unbiased genome-wide analysis suggests that Hsp27 is part of a transcriptional network induced by axonal injury and highly enriched for genes involved in adaptive neuronal responses, particularly regeneration and survival, with relatively few genes responsible for neuronal activity or other cellular functions (25, 28).

**mHsp25 localization.** We have previously shown that Hsp27 is involved in promoting neuronal survival in the adult after nerve injury (16), and we are now interested in defining its potential role in regeneration. Supporting such a possible role, we found that the mouse homolog of Hsp27 (mHsp25) is distributed to the growing edge of growth cones in cultured primary sensory DRG neurons, extending to the very distal tip of F-actin filaments at the barbed end, the site of new actin monomer incorporation (ref. 29 and Figure 2A). Moreover, mHsp25 protein levels increased in the soma (Figure 2D) and in growth cones (Supplemental Figure 1A) after a peripheral nerve lesion that preconditions the sensory neurons to accelerate axonal growth (13).

**mHsp25 loss of function.** To test whether mHsp25 is necessary in the mouse for neurite growth, we knocked down the protein using lentiviral delivery of a shRNA targeted against mHsp25 (shRNA<sup>mHsp25</sup>) to cultured adult DRG neurons. Neurons were transduced with either lenti-shRNA<sup>control</sup> or lenti-shRNA<sup>mHsp25</sup> for 24 hours after dis-

sociation and then grown further for 6 days. On day 7, the neuron cell bodies were separated from their neurites by trypsinization and pipetting, replated, and allowed to grow for a further 17 hours. GFP subcloned into the viral vector revealed a high transduction efficiency ( $81.2\% \pm 1.4\%$ ) (Figure 2B). Lenti-shRNA<sup>mHsp25</sup> substantially reduced or eliminated mHsp25 immunostaining in the majority of neurons transduced (Figure 2B), indicating effective knockdown. However, the knockdown resulted in an accelerated loss of the transduced DRG neurons (Supplemental Figure 1B), in keeping with its survival function (ref. 14 and Supplemental Figure 1B). To overcome this, we knocked down mHsp25 in DRG neurons from *Bax*<sup>-/-</sup> mice, which do not undergo apoptosis (30). The survival rate in *Bax*<sup>-/-</sup> DRG neurons with successful mHsp25 knockdown was identical to that in C57BL/6 neurons transduced with shRNA<sup>control</sup> (Supplemental Figure 1B), indicating that, in *Bax*<sup>-/-</sup> mice, loss of mHsp25 no longer results in cell death. However, in those neurons in which mHsp25 levels were reduced by the shRNA<sup>mHsp25</sup>, neurite growth was reduced more than 3 fold (Figure 2, B and C). In contrast, neurite growth in *Bax*<sup>-/-</sup> DRG neurons transduced with shRNA<sup>control</sup> was identical to that from C57BL/6 WT mice (Figure 2C).

Phosphorylation of Ser15 (1.9 fold) and Ser86 (3.7 fold) of mHsp25 occurred after sciatic nerve injury (Figure 2D), allowing for a second loss-of-function strategy: blocking mitogen-activated protein kinase-activated protein kinase 2 (MK2) (31), the kinase downstream of p38 required for phosphorylation of mHsp25, and its involvement in actin polymerization (20, 22). We found that an MK2 peptide inhibitor that reduced the phosphorylation of mHsp25 also decreased DRG neurite length in a dose-dependent manner (Figure 2, E and F).

**Forced expression of hHsp27 increases axonal growth *in vitro* and *in vivo* in mice.** To examine whether Hsp27 is sufficient to increase axonal growth, we produced 4 Tg mouse lines in which human Hsp27 (hHsp27) is expressed postnatally in neurons under control of the Thy1.2 promoter (Figure 3A). We used hHsp27 so that we could distinguish the transgene from the endogenous mHsp25 (Figure 3, B and G). Expression of the transgene was identified by an antibody against hHsp27, which did not cross-react with mHsp25 in WT littermates (LMs) (Figure 3, B and G). High expression of hHsp27 was detected in the majority of noninjured DRG neurons in all the mouse lines (Figure 3B). In 2 lines, expression was restricted in the peripheral nervous system to sensory neurons (referred to herein as sensory lines), and, in 2 others, both sensory and motor neurons expressed the transgene (referred to herein as motor lines). hHsp27 was localized at the very tip of the growth cone in DRG neurons (Figure 3, C and D), just like endogenous mHsp25, and, in noninjured L4/L5 DRG neurons, hHsp27 Ser78 and Ser82 were constitutively phosphorylated and became more so after sciatic nerve injury (1.8 fold) (Figure 3E). Noninjured Tg mice did not display any detectable difference in baseline sensory or motor function from WT mice (data not shown). We conclude that because hHsp27 is heavily expressed and phosphorylated in noninjured neurons in the Tg mice, these animals can be used to examine whether hHsp27 increases the intrinsic growth capacity of neurons.

To examine this, we prepared dissociated adult DRG cultures from hHsp27 Tg mice and their WT LMs and measured neurite length after 17 hours (Figure 3, F–H). This early time point was chosen because it is before endogenous mHsp25 protein levels increase in response to the axonal injury inherent in the culture (14), and it is a time when a preconditioning priming effect on

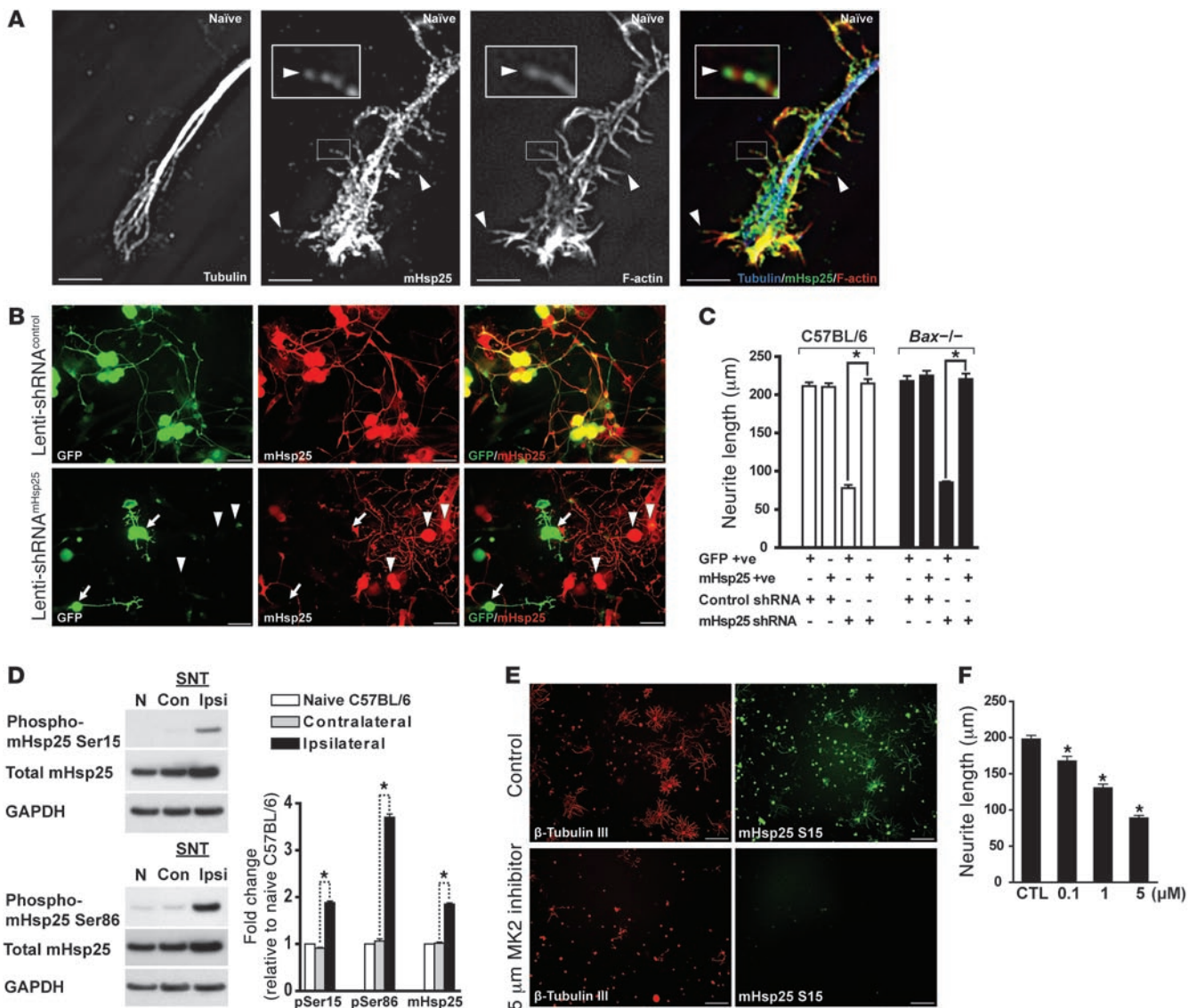


**Figure 2**

mHsp25 colocalizes with actin in growth cone filopodia, and both its knockdown and inhibition of phosphorylation reduce neurite growth. (A) High levels of mHsp25 are present in growth cones of adult DRG neurons, colocalizing with actin at the barbed end tips of filopodia (white arrowheads). Scale bar: 7.5 μm. Original magnification, ×250 (insets). (B) DRG neurons were transduced with lentiviral vectors containing a GFP reporter and either shRNA<sup>control</sup> or shRNA<sup>mHsp25</sup>, and somata were stripped from their neurites after 7-day culture, replated, and allowed to grow for 17 hours. Knockdown of mHsp25 (GFP +ve, mHsp25 –ve; white arrows) reduced neurite length compared with that of nontransduced (GFP –ve, mHsp25 +ve; white arrowheads) neurons in the same culture or with neurons transduced with lenti-shRNA<sup>control</sup>. Scale bar: 50 μm. (C) mHsp25 knockdown reduced neurite length of DRG neurons in C57BL/6 mice (where cell death increased) and *Bax*<sup>-/-</sup> mice (where cell death was prevented; Supplemental Figure 1B). (D) Total Hsp25 protein levels and phosphorylation on Ser15 and Ser86 increased in L4/5 DRGs 3 days after an ipsilateral (ipsi) SNT compared with those in contralateral (con) DRGs. Quantification of Western blots shows relative changes in mHsp25 and its 2 phosphorylation sites (fold change is relative to uninjured naive mice; mean ± SEM of triplicates; \**P* < 0.001, Student's *t* test). (E and F) A peptide MK2 inhibitor that blocks phosphorylation of mHsp25 dose dependently reduced neurite growth (mean ± SEM of triplicates; \**P* < 0.001, 1-way ANOVA followed with post-hoc Newman-Keuls test in C and F). CTL, control. Scale bar: 250 μm.

neurite outgrowth is readily detectable (13). When DRG neurons that constitutively express hHsp27 were compared within the same culture to those that do not, hHsp27 neurons showed a marked increase in neurite number and length (Figure 3, F–H) to an extent similar to that produced by a preconditioning nerve lesion (Figure 3I).

To test whether axonal growth was also enhanced in vivo, we performed a sciatic nerve crush lesion and measured the extent of axonal regeneration distal to the lesion at 72 hours, using GAP-43 to immunolabel regenerating axons (Figure 4A) and the nerve pinch test (12, 13) (see Methods). The number of Gap-43-positive fibers 4.5-mm distal to the crush site was significantly higher in

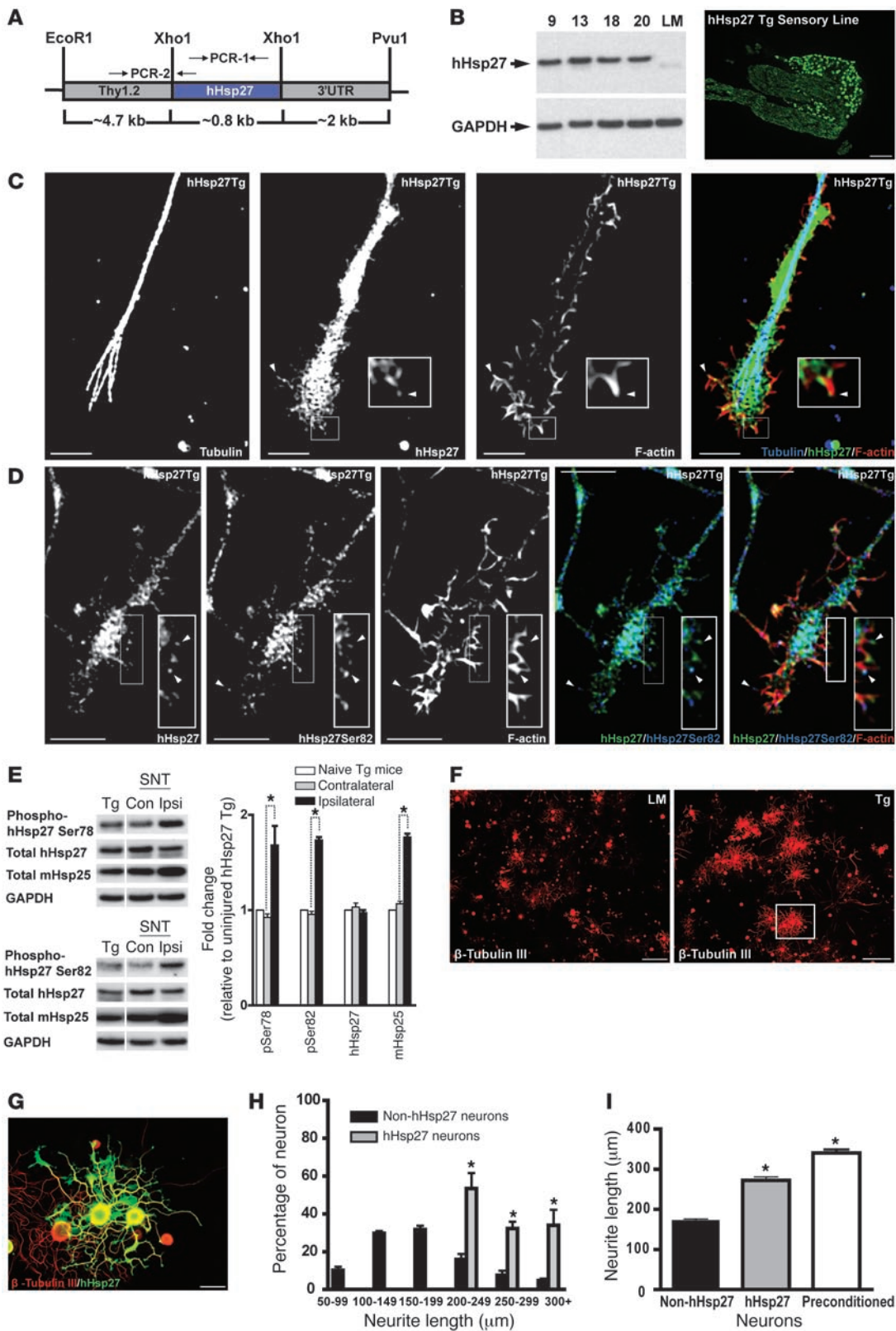




### Figure 3

Forced expression of hHsp27 accelerates axonal growth in vitro. (A) A neuronal specific Thy1.2 promoter was used to generate hHsp27 Tg mice. PCR-1 and PCR-2 represent primer pairs for genotyping. (B) A hHsp27 transgene was expressed at high levels in uninjured adult lumbar DRGs in 4 lines (lines 9, 13, 18, and 20) but was undetectable in WT LMs, measured by Western blot and immunohistochemistry. Scale bar: 250  $\mu\text{m}$ . (C) hHsp27-expressing DRG neurons were immunostained with anti-tyrosinated  $\alpha$ -tubulin (blue), anti-phalloidin for F-actin (red), and anti-hHsp27 (green); white arrowheads indicate the tips of filopodia. Scale bar: 7.5  $\mu\text{m}$ . Original magnification,  $\times 250$  (insets). (D) Phosphorylated hHsp27 (Ser82; blue) colocalized with F-actin at the tips of filopodia (white arrowheads). Scale bar: 7.5  $\mu\text{m}$ . Original magnification,  $\times 250$  (insets). (E) Changes in hHsp27 and phosphorylation on Ser78 and Ser82 were examined in L4/5 DRGs 3 days after SNT in hHsp27 Tg mice. hHsp27 total protein levels did not change from the high constitutive levels, but phosphorylation increased further after injury. Membranes were stripped and reblotted with anti-hHsp27 or anti-mHsp25 for total Hsp (mean  $\pm$  SEM of triplicates;  $*P < 0.01$ , Student's *t* test). The lanes were run on the same gel but were noncontiguous. (F) WT LM DRG neurons possess shorter neurites than hHsp27 Tg mice. Scale bar: 250  $\mu\text{m}$ . (G) Magnified view from white box in F. hHsp27-expressing neurons (yellow) and non-hHsp27-expressing neurons (red) are distinguishable by double labeling for tubulin (red) and hHsp27 (green). Scale bar: 16.7  $\mu\text{m}$ . (H) Size frequency analysis of neurites in hHsp27 Tg cultures, showing increased length in hHsp27 neurons. (I) The growth-promoting effect of hHsp27 is comparable to the preconditioning effect (SNT 1 week before culture) (mean  $\pm$  SEM of triplicates;  $*P < 0.001$ , 1-way ANOVA, followed with post-hoc Newman-Keuls test in H and I).

hHsp27 Tg mice than that in their LMs (Figure 4B). The distal extent of sensory axonal growth at 72 hours detected by the pinch test almost doubled in 2 independent hHsp27 Tg mouse lines compared with that in LMs (1.6 and 1.7 fold) (Figure 4C). Furthermore, the MK2 peptide inhibitor reduced the enhanced growth of hHsp27-expressing DRG neurons in vitro (Supplemental Figure 2) and the extent of sensory axonal regeneration in vivo (Figure 4D).

These data collectively show that mHsp25 appears to be necessary for axonal growth in adult DRG neurons and that expression of hHsp27 in noninjured sensory neurons is sufficient to prime them for accelerated axonal growth immediately after an injury.

*hHsp27 enhances sensory and motor functional recovery after sciatic nerve transection.* We next wished to determine whether the hHsp27 sensory Tg lines (with no hHsp27 expression in motor neurons) display accelerated recovery of peripheral cutaneous sensitivity after nerve injury. We assessed the recovery of nociceptive sensitivity in the mice by applying a pinprick to the distal skin territory of the injured sciatic nerve (lateral hind paw) at various times after the injury. After a sciatic nerve crush, WT LM mice showed some restoration of nociceptive sensitivity in the skin of the lateral paw, beginning at 10 to 12 days, a situation that was significantly accelerated in hHsp27 Tg mice (9–10 days) (Figure 5A). After a transection of the sciatic nerve with immediate resuture, WT LMs showed a slower (17–18 days) recovery of sensation that was also accelerated in hHsp27 Tg mice (13–15 days) (Figure 5A). The numbers of NF-200-positive axons in the sciatic nerve 5- to 20-mm distal to the transection injury site at 1 week were significantly higher in hHsp27 mice than in WT mice (Figure 5, B and C).

In the 2 Tg lines constitutively expressing hHsp27 in motor neurons (Figure 6A), we were able to test whether hHsp27 also increases motor recovery after axonal injury. Recovery of motor function in

the toes (measured by the toe spreading reflex, a measure of plantar muscle function, and gait) after a sciatic nerve crush injury was significantly accelerated in mice that expressed the transgene in motor neurons (Figure 6B and Supplemental Figure 3A) but not in those lines that expressed the transgene only in sensory neurons (Supplemental Figure 3B). Although WT LM mice did show full restoration of motor function within 21 to 26 days of a sciatic nerve crush lesion (Figure 6B and Supplemental Figure 3B), recovery of motor function in the paw after a sciatic transection/resuture injury was effectively almost absent in these mice, with minimal return in toe spreading over 8 weeks of observation (Figure 6, B–D). In WT LM mice, the foot remained clawed, immobile, and paralyzed, with significant muscle atrophy (Supplemental Figure 4A) and contracture (Supplemental Figure 4B). In contrast, hHsp27 motor neuron Tg mice showed a progressive improvement in motor recovery (Figure 6, B–D), reduced muscle atrophy (Supplemental Figure 4A), and no contracture (Supplemental Figure 4B). We replicated the recovery of motor function and accelerated sensory recovery in independent Tg lines (Supplemental Figure 4, C and D).

*hHsp27 increases reinnervation of the motor end plate.* No difference in the size or disposition of scar at the site of transection/resuture nerve injury was found between WT and hHsp27 Tg mice (Supplemental Figure 5). While at 1 week we found reduced axonal growth distal to the transection lesion in WT LMs compared with that in hHsp27 mice (Figure 5B), reflecting accelerated growth in the hHsp27 mice, there were essentially identical numbers of axons in both the sciatic (Figure 6, E–G) and distal tibial nerves (Figure 6H) 8 weeks after the lesion in WT LMs and hHsp27 Tg mice. This indicates that eventually axonal growth in WT mice catches up to that in the Tg mice and, in both groups of mice, regenerating axons reach distal nerves. Survival of motor neurons was also identical in hHsp27 Tg mice and WT LMs 8 weeks after the sciatic nerve transection (SNT) injury (Supplemental Figure 6A).

In WT LMs only 20% of motor end plates in the abductor digiti minimi lateral plantar muscles were reinnervated by neurofilament positive axons after the sciatic transection/restoration injury. However, the extent of reinnervation of the motor end plates in these muscles fully recovered at 8 weeks to uninjured levels in the hHsp27 Tg mice (Figure 7A), and this was replicated in an independent Tg motor line (Figure 7B). In spite of the failure of motor end plate reinnervation in WT LM mice, many axons were present within muscle nerve fascicles, in keeping with the normal axon counts in the distal tibial nerve (Figure 6H), and these were choline acetyltransferase positive (Supplemental Figure 7). These axons approached but either did not enter the motor end plate or only had minimal branching within it and did not form synaptophysin-labeled presynaptic terminals (Figure 7B). In contrast, the axonal innervation pattern of the end plate in hHsp27 Tg mice 8 weeks after the transection/resuture injury looked effectively identical to those in noninjured mice, including normal neurofilament and synaptophysin label in the end plate (Figure 7). In both the WT LMs and hHsp27 Tg mice S100-positive terminal Schwann cells were present within the end plate (Supplemental Figure 8).

*A critical period for motor functional recovery in mice and humans after nerve injury.* An analysis of our whole data set revealed that recovery of function the plantar muscles in individual mice plateaued at around 35 days, with minimal further recovery beyond this (Figure 8A). This suggested to us that there may be a limited time window when regenerating axons can reestablish contact with denervated

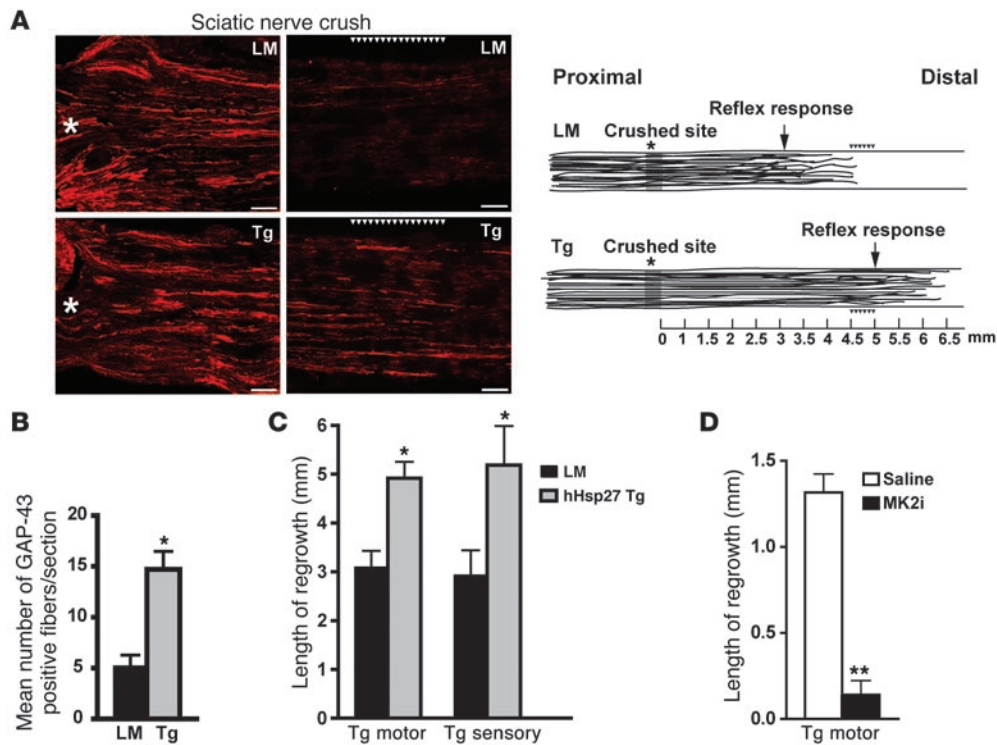


**Figure 4** hHsp27 overexpression accelerates axonal growth after nerve crush in vivo. (A) Gap-43 immunoreactivity was used to determine the extent of axonal regeneration 72 hours after a sciatic nerve crush injury in WT LMs and hHsp27 Tg mice 4.5 mm from the crush site (indicated by \*). Scale bar: 100  $\mu$ m. Schema of representative LM and Tg sciatic nerves, showing results of (B) Gap-43 immunoreactivity and (C) pinch test. Gap-43 fibers were quantified between 4.5 to 5 mm from the crush site. (B) hHsp27 Tg mice had more Gap-43 immunoreactive fibers per section compared with LMs ( $n = 3-5$  per group;  $*P < 0.001$ , Student's  $t$  test). (C) Sensory fiber regeneration, determined by the pinch test was significantly enhanced in hHsp27 Tg mouse lines that express hHsp27 in DRGs compared with that in LM controls ( $n = 10-12$  per group;  $*P < 0.05$ , Student's  $t$  test). (D) An intraneural injection of a peptide MK2 inhibitor (MK2i) (10  $\mu$ M) was made distal to a sciatic nerve crush site in hHsp27 Tg mice, and the pinch test was performed 32 hours later. Axonal regeneration was decreased significantly in the MK2 inhibitor-treated groups ( $n = 6$  per group;  $**P < 0.001$ , Student's  $t$  test).

ed end plates and that the slow regeneration in WT mice after a transection/resuture injury might be responsible for the failure to restore neuromuscular junctions (NMJs). We hypothesized that by the time WT motor axons eventually arrive at the motor end plate after a transection it may no longer be permissive for reinnervation. To test this possibility, we performed repeated sciatic nerve crushes in WT mice to prevent axons from reaching the muscle for 2 different periods (Figure 8B). Sciatic nerves were crushed 4 times at 2-day intervals (short denervation period, preventing reinnervation for 16 days) and at 9-day intervals (long denervation period, preventing reinnervation for 37 days) in C57BL/6 mice. Motor function (toe spreading) recovered completely in the repeated short- but not long-term crush mice (Figure 8B), which indicates that reinnervation of the target motor end plate in plantar muscles before 5 weeks (Figure 8A) appears essential for functional recovery in the mice. In stark contrast, an equivalent degree of sensory recovery occurred in both of the repeated crush groups. We conclude that while sensory recovery can occur after a prolonged sensory denervation, there may be a critical period after denervation when the motor end plate remains permissive for the reformation of the presynaptic terminal (Figure 8A), after which reinnervation is either limited or absent.

In an attempt to assess whether these findings reflect what happens in humans after peripheral nerve injury, we examined sensory and motor recovery in a group of patients operated for entrapment neuropathy due to carpal tunnel syndrome (CTS) ( $n = 136$ ) or cubital tunnel syndrome (CuTS) ( $n = 20$ ). All patients with CTS recovered sensation, based on questionnaires, and all patients with CuTS who lacked distal sensory or motor function at the time of surgery regained a degree of sensation after the surgical decompression, as evaluated by mechanical threshold (Figure 8C). However, motor recovery measured by compound muscle action potentials and manual muscle testing was generally poor and, in some patients, absent (Figure 8D). Interestingly, for both the patients with CTS and CuTS with complete denervation of target muscle, the shorter the period from onset of symptoms to surgery, the greater the degree of motor recovery (Figure 8E), supporting the possibility of a limited time period when functional NMJs can be restored sufficiently to recover function. Nevertheless, the window for motor recovery appears to be much longer in humans than in mice. These clinical data suggest that while regeneration in sensory axons can, after even prolonged nerve damage, restore skin sensation, motor function fails to be reestablished to a similar extent in most patients.

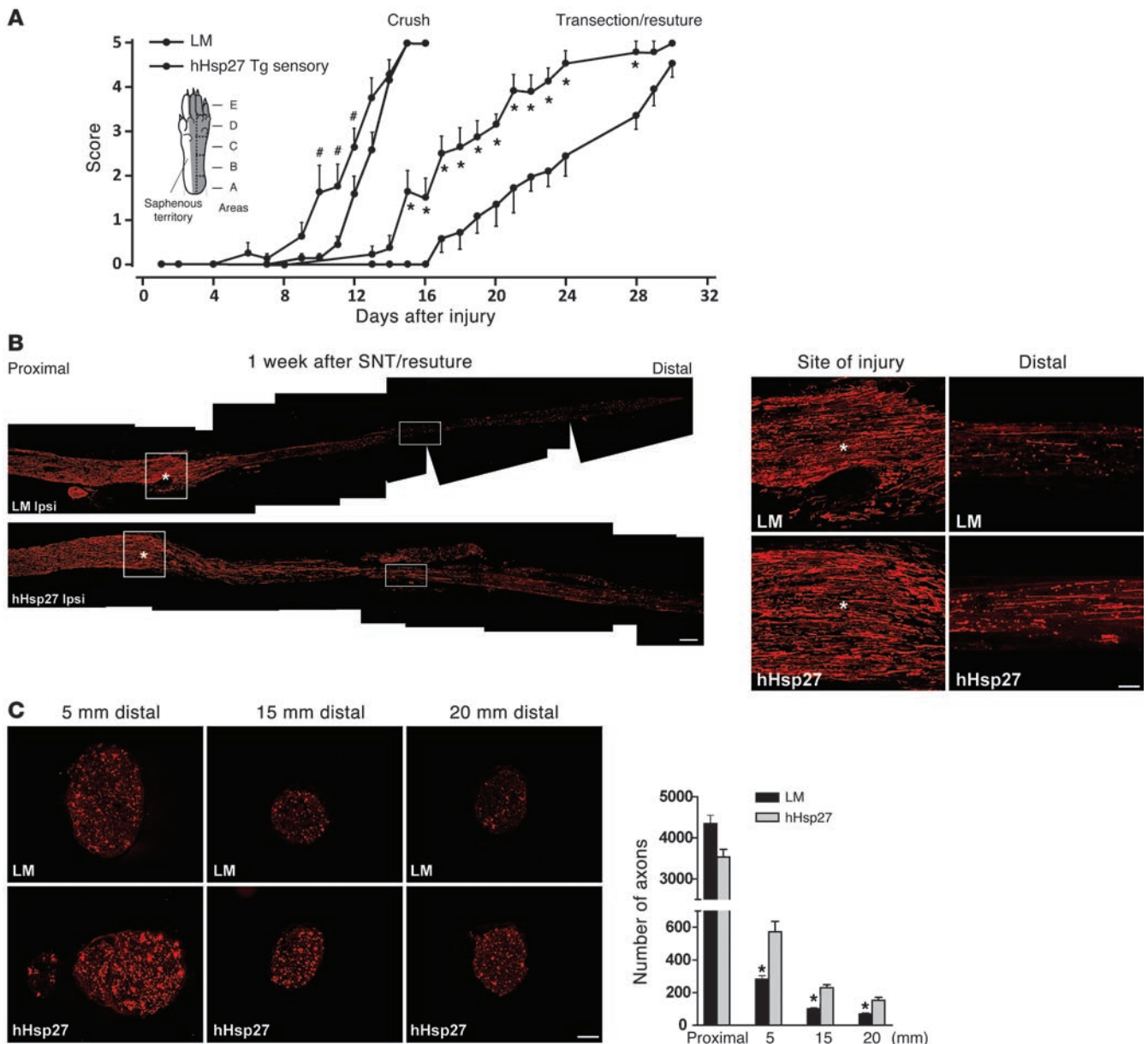


**Figure 5**

hHsp27 enhances functional sensory recovery after sciatic nerve crush and transection/resuture injury. **(A)** Sensory recovery, assessed by response to pinprick stimulation (see Methods), showed earlier reinnervation of the whole paw in hHsp27 sensory lines than in WT LM ( $n = 7-8$  per group;  $*P < 0.05$  and  $*P < 0.05$ , 2-way repeated measures ANOVA, with post-hoc Bonferroni analysis). **(B)** Longitudinal sections of sciatic nerve immunostained for neurofilament 1 week after transection/resuture show faster axonal regrowth in hHsp27 Tg mice. Multiple serial micrographs were captured and tiled into a single composite image. Scale bar: 500  $\mu\text{m}$ . Magnified views from the boxed areas are shown in the right panel. Scale bar: 50  $\mu\text{m}$ . **(C)** Quantification of the total number of axons in 4- $\mu\text{m}$ -thick transverse sciatic nerve sections immunostained for neurofilament ( $n = 4-6$  per group;  $*P < 0.001$ , 1-way ANOVA followed with post-hoc Newman-Keuls test). Scale bar: 50  $\mu\text{m}$ .

**Discussion**

Neural regeneration requires detection of axonal injury by retrograde signaling from the injured site to the cell body in order to induce those genes whose activity is necessary for the initiation, formation, elongation, and guidance of growing axons as well as reformation of specialized contacts with targets. Most growth-associated proteins are induced in the soma and transported orthogradely to the growth cone, but several transcripts are also translated locally in the axon,

including Hsp27 (32). Some growth-associated proteins constitute the actual cytoskeletal molecular machinery necessary for extension of growth cones (31, 33) while others enable growth cones to interact with guidance cues in the environment to regulate the rate and direction of growth (34) and may also detect growth inhibitory cues.

While axonal growth after nerve injury in the adult may recapitulate some of the processes used during the development of the nervous system, they are not mechanistically identical (35). Unlike

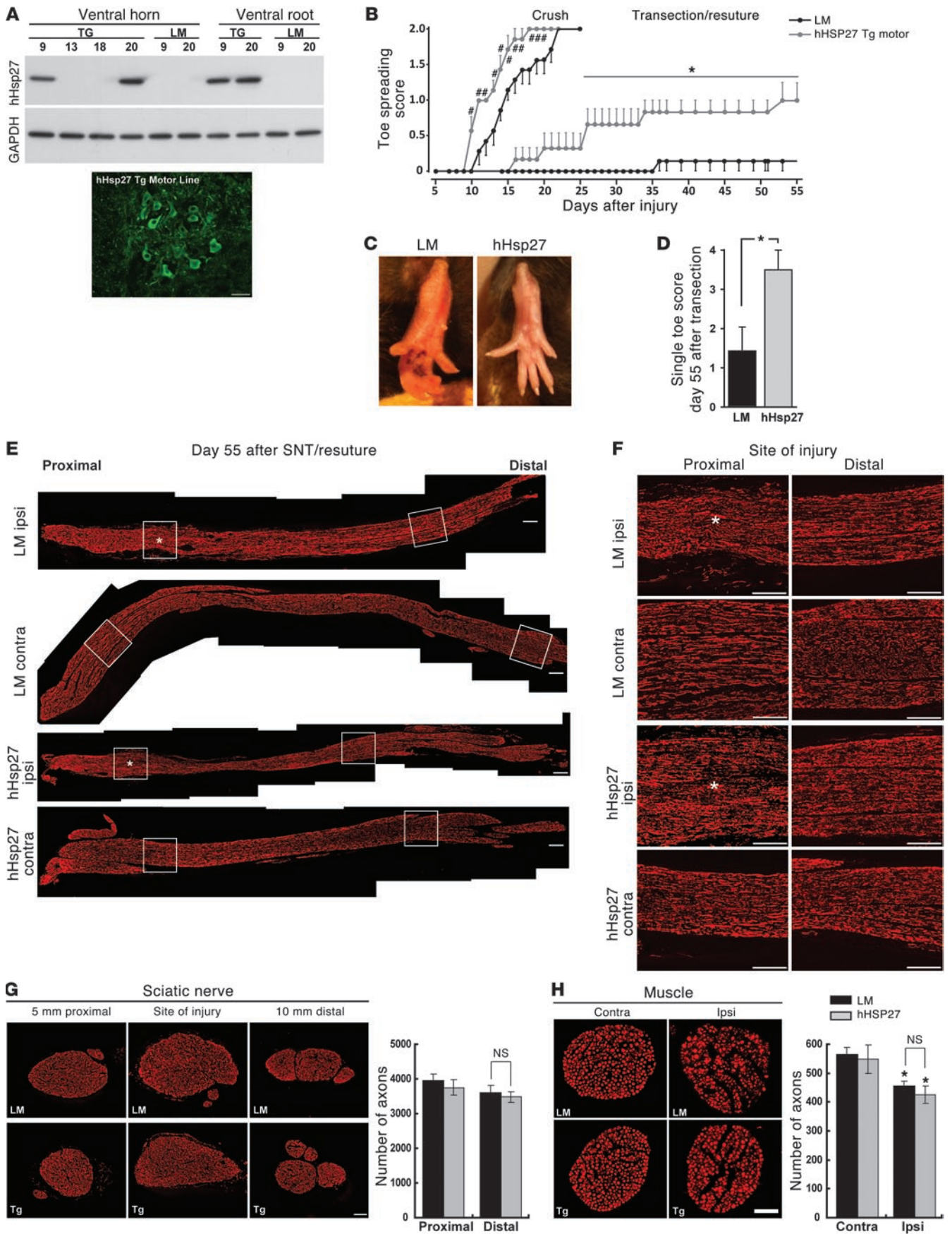


**Figure 6**

hHsp27 promotes functional motor recovery and quantification of axon number in the sciatic nerve 55 days after transection/resuture. **(A)** hHsp27 transgene was detected by Western blot in uninjured adult ventral horn/root in motor lines (lines 9 and 20) but not in sensory lines (lines 13 and 18), and hHsp27 was highly expressed in ventral horn motor neurons in motor lines. Scale bar: 50  $\mu\text{m}$ . **(B)** hHsp27 Tg motor lines showed a marked improvement in toe spreading reflex ( $n = 6\text{--}7$  per group;  $\#P < 0.01$  and  $*P < 0.01$ , 2-way repeated measures ANOVA, with post-hoc Bonferroni analysis). **(C)** Clear toe spreading was evident in hHsp27 Tg mice 55 days after transection/resuture. **(D)** Number of toes that actively spread in LMs and Tg mice after injury ( $*P < 0.05$ , Student's *t* test). **(E)** Axonal (neurofilament +ve axons) regrowth is similar in both groups. Multiple serial micrographs were captured and tiled into a single composite image. Contra, contralateral. Scale bar: 500  $\mu\text{m}$ . **(F)** Magnified views from the boxed areas in **E**. The asterisks indicate injury sites. Scale bar: 100  $\mu\text{m}$ . **(G)** No significant differences in neurofilament +ve axons between groups were detected in the ipsilateral side of sciatic nerves after injury ( $n = 4\text{--}6$  per group;  $P < 0.05$ , Student's *t* test). Scale bar: 50  $\mu\text{m}$ . **(H)** There were fewer neurofilament +ve axons in the gastrocnemius branch of tibial nerve on the ipsilateral side relative to those on the contralateral side, but this was not significantly different between groups ( $n = 5$  per group;  $*P < 0.001$ , 1-way ANOVA followed with post-hoc Newman-Keuls test). Scale bar: 20  $\mu\text{m}$ .

mammalian CNS neurons, primary sensory and motor neurons can regenerate after axonal injury in the adult, and this provides an opportunity for identifying which injury-induced genes are necessary and the nature of permissive growth environments. These neurons can be primed into an active growth state by a preconditioning peripheral nerve lesion (10, 36), after which the rate and extent of axon formation is greatly increased as a result of induction by the preinjury of the proteins required for growth. Our data now suggest that Hsp27 plays a major role in enabling axons to grow and in the conditioning effect.

Hsp27 was identified by its capacity to promote survival in heat-stressed cells (37). In addition to a classic chaperone function, which contributes to its actions after heat shock, Hsp27 interacts with proapoptotic proteins to reduce apoptosis (38), a function it also subserves in injured adult sensory and motor neurons (16). Hsp27 regulates actin dynamics and contributes thereby to cell motility, migration, contraction (19, 22), and, as we now show, axonal elongation. This actin-interacting role involves Hsp27 cycling from its dephosphorylated to its phosphorylated form through p38 MAPK (19), for which Hsp27 is a major substrate (20), and our data indicate that inhibition of MK2 is sufficient to block the growth-promoting effects of Hsp27 in vitro and in vivo.

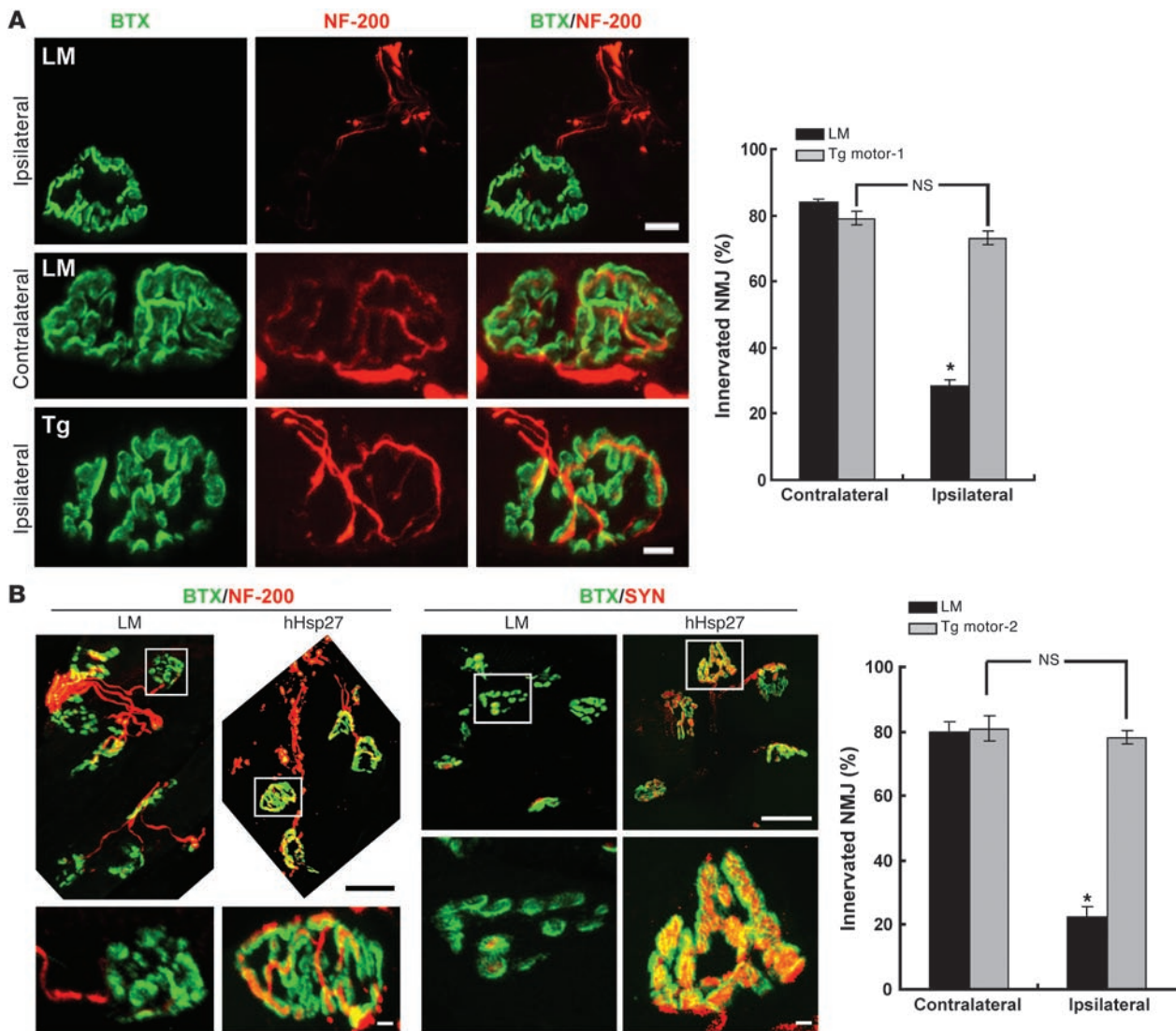
mHsp25 is induced in injured sensory neurons, and its phosphorylated form is present at the tip of filopodia, the sole site of actin monomer addition in growth cones. Therefore, Hsp27 is well positioned anatomically to regulate filopodial cytoskeletal dynamics and facilitate growth cone locomotion during regeneration. We demonstrate that forced expression of hHsp27 in uninjured mouse neurons increased intrinsic axonal growth and that it may also be required for such growth as indicated from mHsp25 knockdown. Our data point to a pivotal role for Hsp27 in increasing the intrinsic growth of injured sensory neurons and show that its expression accelerates the rate of functional reinnervation of injured sensory neurons in damaged peripheral nerves.

Peripheral nerve injury results in a massive alteration in transcription (11) mediated by activation of several transcription factors, *Atf3*, *c-Jun*, *Stat3*, and *Sox11*, all of which increase regeneration (13,

39–41). These genes also contribute to overcoming the metabolic stress of the axonal injury, promote cell survival by inhibiting apoptosis, and alter membrane excitability and synaptic transmission as well as promoting axon regrowth (13, 39, 42). What is not clear, though, is whether these functional changes are independently regulated. We found that the genes most highly coassociated with the regulation of Hsp27 are highly enriched for growth and antiapoptotic functions, with few candidate neuropathic pain genes, suggesting that the genes upregulated or downregulated after nerve injury are linked into functionally coherent modules or networks.

Increasing the intrinsic growth status of injured neurons, although necessary for successful regeneration is not by itself sufficient. Neurons also need a permissive growth environment, such as that provided in peripheral nerves by Schwann cells and laminin (4). However, permissive growth environments also are by themselves not adequate for regeneration, because most unprimed neurons do not have enough intrinsic growth capacity to drive full regeneration (43, 44). Furthermore, if distal nerve segments lose Schwann cells, as occurs after chronic denervation of distal nerves for many months, this provides limited support for axonal growth, and regeneration is reduced or halted (45–47). The extent of motor recovery in the rat reduces over time after chronic denervation, and early nerve repair is required for muscle strength to return (8). Although this finding aligns with our data, it was assumed to be the effect of decreased axonal regeneration in the nerve distal stump due to Schwann cell atrophy after prolonged denervation (8, 47), while our data from the plantar muscles of the mouse points to another more specific defect, failure of reinnervation of the motor end plate.

Recovery after injury of peripheral nerves in humans is more limited than in rodents, because the distance to the target is longer and the intrinsic axonal growth rate is slower (48). Major factors recognized as influencing the outcome of peripheral nerve repair are the degree of injury, the age of the patient, type of nerve, level of injury, and the timing of repair, the last of which is particularly related to our findings. Proximal injuries, such as brachial plexus injuries, show only very limited motor recovery for wrist and finger flexors and none for intrinsic muscles (5, 49). Delay in surgery of over 6 months significantly reduces the extent of motor recovery, and it is considered clinically fruitless to expect motor recovery if an operation is delayed for more than a year (50). However, sensation commonly recovers even though the quality may be defective, pointing to a clear difference in functional sensory and motor recovery. Ninety percent of patients with brachial plexus injury, for example, recover protective sensation in their fingers in the absence of any meaningful recovery in thenar muscles (49). This agrees well with our data, showing substantial sensory but only minimal motor recovery after a SNT injury. We show, in addition, data suggestive of a critical period of 10 to 12 months in patients for recovery of motor function after denervation, while in the mouse we found the cut off for plantar muscles to be 4–6 weeks. Several mechanisms could potentially be responsible for the failure of reinnervation of the motor end plate that we found for plantar muscles in mice after a critical period of 5 to 6 weeks (Figure 7 and Figure 8A). The first could be a loss or reduction in the intrinsic growth capacity of injured motor neurons over time, such that growth of their axonal tip ceases before they reach the end plate. This seems unlikely, however, since motor neurons appear to be capable of axonal elongation even after prolonged periods of time, provided the milieu is permissive (46, 51, 52). In addition, we found that motor axons after a transection injury in

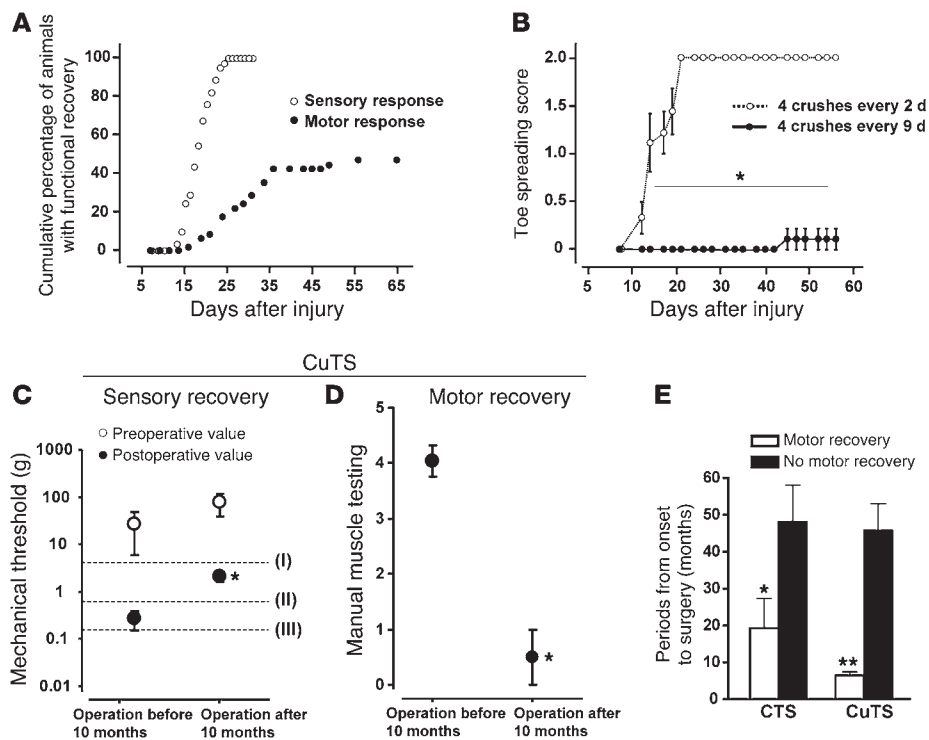


**Figure 7**

hHsp27 promotes restoration of motor end plate innervation after SNT/resuture injury. **(A)** Confocal images of the NMJ in hHsp27 Tg mice and WT LMs. Neurofilament (NF-200; red) and bungarotoxin (BTX; green) immunostaining shows little NMJ reinnervation in ipsilateral plantar muscles of LM controls 55 days after injury, even though axons are in nerve branches and approach the end plate. In contrast, ipsilateral hHsp27 plantar muscles show a reinnervation comparable to levels on the contralateral uninjured side ( $n = 6$  per group;  $*P < 0.001$ , 1-way ANOVA with post-hoc Newman-Keuls test). Scale bar: 10  $\mu\text{m}$  (top row); 5  $\mu\text{m}$  (middle and bottom rows). **(B)** NMJ reinnervation was confirmed in a second independent hHsp27 Tg motor line with the synaptic vesicle marker synaptophysin (SYN) in addition to NF-200. Graph showing quantification of the innervation of plantar muscle NMJ ( $n = 6$  per group;  $*P < 0.001$ , 1-way ANOVA with post-hoc Newman-Keuls test). Scale bar: 20  $\mu\text{m}$  (top row); 5  $\mu\text{m}$  (bottom row).

WT mice eventually do grow in locations immediately adjacent to the end plate, so that they only would need a few microns of additional growth to complete the reinnervation. Furthermore, we found that sensory axons are capable of reinnervating even the most distal skin areas. Another possibility is that Schwann cells in denervated motor nerves become nonpermissive or even repellent to axon growth over time (47) so that regenerating axons halt when they reach such denervated nerves (53–55). Because we found many axons in the most distal muscle nerves in WT mice after a sciatic transection, we think this is unlikely at the time window we are looking at (~8 weeks); the nerves appear to be fully

permissive for axonal regeneration, although they may certainly become less permissive at longer periods of denervation (9, 46). Our hypothesis is that the terminal Schwann cell in the end plate may become nonpermissive for axonal growth after prolonged denervation. Soon after denervation, these specialized cells, which are normally in contact with the axon up to the synaptic cleft, dedifferentiate and elaborate processes that spread away from the synaptic zone (56) and then fully recover to the uninjured phenotype after reinnervation after crush injuries (57). The terminal Schwann cell processes extending from denervated end plates act as substrates for axonal growth, assisting both reinnervation and

**Figure 8**

Timing is crucial for functional motor recovery in mice and humans after nerve injury. **(A)** Cumulative percentage of animals (WT and Tg) with functional recovery after SNT/resuture. Functional recovery was defined as the first day the mice exhibited a positive response in pinprick (sensory response,  $n = 14\text{--}21$  per group from 2 sensory lines) or toe spreading tests (motor response,  $n = 13\text{--}26$  per group from 2 motor lines). **(B)** When the sciatic nerve was crushed 4 times with a 2-day interval (16 days of denervation), mice showed a full recovery in the toe spreading reflex. In contrast, when the crushes were performed 4 times with a 9-day interval (37 days of denervation), recovery was markedly reduced ( $n = 9$  per group;  $*P < 0.0001$ , 1-way ANOVA with post-hoc Newman-Keuls test). **(C)** Sensory recovery in patients with CuTS. White circles represent the preoperative, and black represent the postoperative, mechanical threshold on the distal phalanx of the little finger. The dash lines represent the border between loss of protective sensation (I), diminished protective sensation (II), and diminished light touch (III) ( $n = 20$ ;  $*P = 0.0012$ , Student's  $t$  test). **(D)** Relationship between duration of symptoms and motor recovery in patients with CuTS. A value of 5 on the  $y$  axis represents normal muscle strength, and a value of 0 on the  $y$  axis represents complete denervation ( $n = 20$ ;  $*P = 0.000029$ , Student's  $t$  test). **(E)** Comparison of duration from onset to surgery in patients operated with complete target muscle denervation in CuTS ( $n = 20$ ) and CTS ( $n = 136$ ) ( $*P < 0.05$ ;  $**P < 0.0001$ , Student's  $t$  test).

collateral sprouting (58). However, the number and phenotype of terminal Schwann cell can decrease with prolonged denervation (59). A lack of terminal Schwann cells, their processes, or of the trophic and guidance molecules they express, such as TGF- $\beta$ , agrin, or CNTF (58, 60), may contribute to reduced reinnervation. Because we found terminal Schwann cells still present in the end plate in WT mice with no reinnervation, we concluded that the failure of regrowth is not due to a simple loss of these cells at this duration of denervation. Terminal Schwann cells may begin to produce growth inhibitory molecules like Sema 3A or chondroitin sulfate proteoglycan (61, 62), which could block axonal growth into this site. Finally, it is well known from developmental studies that the formation of a functional synapse at the NMJ depends on a fine orchestration of signaling pathways between the nerve and the muscle. Regenerating nerve terminals may require a positive trophic signal, such as FGF, GDNF,  $\beta_1$  integrin, or synaptic collagens (63), from the muscle to complete formation of the end plate, and this may diminish with denervation over extended periods of time. Future experiments are required to tease out why motor axons do not reestablish synaptic contact with muscles after a critical period of denervation.

We conclude that accelerating axonal growth by overexpressing a single gene that increases actin polymerization in growth cones can increase the rate of sensory recovery and substantially restore motor function after a complete transection/resuture of a peripheral nerve. This finding contrasts with the situation in WT mice, in which there is little return of motor function in plantar muscles after this injury, even though their slowly growing motor axons eventually reach within a few microns of the motor end plate. Surprisingly, failure of successful regeneration in this model is not due, therefore, to an absence of distal axonal growth or to the finding by axons of pathways in the distal nerve, as previously assumed (9), but rather to the failure of formation of the presynaptic component of the NMJ. Success in recovery of motor function may occur in the hHsp27 mice, because the motor axons reach the motor end plate before this structure becomes nonpermissive for reinnervation. The molecular determinants, in muscle or nerve, responsible for preventing synapse reformation after prolonged denervation need to be established as well as whether limited permissive periods for reinnervation are restricted to these peripheral synapses. Nevertheless, based on our mouse data and clinical observations, we



suggest that strategies that increase the rate of intrinsic growth in motor neurons may enhance functional recovery in patients after peripheral nerve damage.

## Methods

**Surgery.** Animal care was in full accordance with the IACUC guidelines of Children's Hospital Boston. All surgical experiments were performed under 2.5% isoflurane on adult male mice (8 to 12 weeks old). SNT was performed by exposing the left sciatic nerve at mid-thigh level, ligating with 6-0 suture, and transecting distal to the ligature. For sciatic nerve crush injury, the sciatic nerve was crushed with smooth forceps for 15 seconds, and the site of crush was marked with a 10-0 epineural suture (Ethilon). Sciatic nerve anastomosis (resuture) was performed at the level of external rotator muscles, just distal to the sciatic notch. The exposed nerve was transected using ophthalmic microscissors (FST). Two epineural sutures were immediately made after the transection under the light microscope (Leica, M50) with 10-0 nylon sutures (Supplemental Figure 9A). After injury, wound was sutured in layers, and the mice were allowed to recover on heated pads. The surgeon who performed the transection/resuture surgery was blinded to the genotype.

**Microarray analysis.** RNA extraction and chip hybridization were carried out as described previously (11). Spared nerve injury, chronic constriction injury, and spinal nerve ligation injury were each carried out on 3 separate groups of rats. L4 and L5 DRGs ipsilateral to the nerve injury were dissected. Each cRNA probe was prepared using pooled tissues from 5 rats; for each time point, 3 biologically independent hybridizations were performed. The microarray data were deposited in Gene Expression Omnibus (accession GSE30691; <http://www.ncbi.nlm.nih.gov/projects/geo/query/acc.cgi?acc=GSE30691>).

A WGCNA was performed as described previously (25, 64). Briefly, after selecting the genes called present in at least 5 samples, the absolute Pearson correlations between one gene and every other gene were computed, weighted, and used to determine the TO, a measure of connection strength or neighborhood sharing. A pair of nodes in a network is said to have high TO if they are both strongly connected to the same group of nodes. Genes with high TO have been found to have an increased chance of being part of the same tissue, cell type, or biological pathway. Genes were clustered based on TO, and groups of highly interconnected genes (modules) were identified. NNA (19) provides a set neighborhood of an initial set of nodes. The top 30 nearest neighbors were added to the chosen seed (*Hspb1*; Affymetrix probe, *rc\_A1176658\_s\_at*) using TO as a measure of connection strength.

**Primary dissociated DRG cultures.** Dissociated DRG cultures were prepared from adult male mice (12 to 14 weeks old) as described previously (14). For preconditioning DRG cultures, 1 week after SNT, L4 and L5 DRGs, supplying the sciatic nerve, from the ipsilateral and contralateral side of the injury in C57BL/6 mice, were collected separately. DRGs were cultured for 17 hours, fixed, immunostained, and analyzed. Data were obtained from at least 3 separate experiments repeated in duplicate.

**Growth cone imaging.** DRG cultures were fixed with PHEM (60 mM Pipes, 25 mM HEPES, 10 mM EGTA, 8 mM MgSO<sub>4</sub>, pH 7.0) and immunostained for anti-tyrosinated  $\alpha$ -tubulin (1:2,500; Millipore), Alexa Fluor 594-conjugated anti-phalloidin (1:250; Molecular Probes), anti-hHsp27 (1:500; Stressgen), anti-phospho-hHsp27-S82 (1:250; Stressgen), or anti-mHsp25 (1:200; Stressgen). Images were collected using a  $\times 60$  objective on a DeltaVision deconvolution microscope (Applied Precision). Raw images were processed by 2 rounds of deconvolution. Deconvolved images were flattened using quick projection. Chromatic aberration was corrected manually using Photoshop.

**Lentiviral production and infection.** Mission control plasmid containing either shRNA sequences to *Hspb1* (mHsp25, SH1911) or a shRNA control vector (SHC001) containing a nonspecific shRNA were purchased from

Sigma-Aldrich. GFP was subcloned into the pLK0.1-puro. Plasmid CSCGW2 was cut with *Nhe1* and *Kpn1* to obtain the EGFP fragment, which was then subcloned into pLK0.1-puro cut with *Spe1* and *Kpn1*, ablating the *Spe1/Nhe1* site. Viral particles were produced as previously described (65).  $4.5 \times 10^4$  tu/ml shRNA<sup>control</sup> or shRNA<sup>mHsp25</sup> was mixed with 7  $\mu$ g/ml polybrene for 5 minutes prior to use. One hour after plating, the mixture (shRNA plus polybrene) was added to the DRG cultures and incubated for 24 hours. On the next day, an equal amount of fresh medium (1:1) was added to each well. The media were then changed every 3 days. One week after infection, DRG cultures were trypsinated (0.25%) and replated. The DRG cultures were fixed with 4% paraformaldehyde 17 hours after replating. Fixed cells were immunostained for anti-GFP (1:500; Chemicon) and anti-mHsp25 (1:200; Stressgen). Infection efficiency ( $81.2\% \pm 1.4\%$ ) was assessed by counting GFP- and mHsp25-positive neurons in 8 randomly selected microscope fields per well from the shRNA<sup>control</sup>-infected cultures in 3 separated experiments. Measurements were made blinded to treatment.

**Bax<sup>-/-</sup> mice.** Bax<sup>-/-</sup> male mice on a C57BL/6 background (66) were obtained from The Jackson Laboratory. These animals have been backcrossed to the C57BL/6 at least 25 times, making this strain congenic.

**Generation of hHsp27 Tg mice.** A hHsp27 coding sequence (750 bp) was subcloned into the *Xho I* site of the Thy1.2 expression cassette (67). The Thy1.2 expression cassette was provided by Pico Caroni (Friedrich Miescher Institute, Basel, Switzerland). After *EcoRI-PvuII* digestion, the *hHsp27* transgene and expression construct were microinjected into fertilized B6C3F1 mouse oocytes to produce Tg mouse lines. Tg mice were identified by PCR of genomic DNA. Two pairs of primers were used. PCR1-forward 5'-ACGAGCATG-GCTACATCTCC-3' and PCR1-reverse 5'-CGGGCTAAGGCTTTACTTGG-3' were located within the *hHsp27* transgene. PCR2-forward 5'-GTCCTGGAT-GTCAACCACT-3' and PCR2-reverse 5'-GGGTTCTTAGGAGGGACAA-3' include both transgene and *Thy1.2* promoter sequences (see Figure 3A). Founder mice with the hHsp27 transgene were crossbred with C57BL/6 mice to establish Tg lines. F<sub>7</sub>-F<sub>9</sub> generations of offspring were used. The Tg mice were fertile and viable and did not show any abnormal phenotype.

**Neurite outgrowth assay.** MK2 inhibitor peptide (WLRRIKAWLRRIKALN-RQLGVAA) was synthesized at the Massachusetts General Hospital Peptide Core Facility. 1,500 cells were plated per well (the MK2 inhibitor was added to the cultures), which were allowed to grow for 17 hours, and fixed with 4% paraformaldehyde. Fixed cells were immunostained with anti- $\beta$ -tubulin III (1:800; Sigma-Aldrich), anti-mHsp25 S15 (1:300; Stressgen), and/or anti-hHsp27 (1:500; Stressgen) accordingly and then with Alexa Fluor 488- or Alexa Fluor 594-conjugated secondary antibody (1:500; Molecular Probes). The longest neurite per neuron was measured using ImageJ software (<http://rsbweb.nih.gov/ij/>). Data were from 3 separate experiments using 2 eight-well chambers for each experiment. At least 800 cells per well were analyzed, blinded to treatment or genotype.

**DRG cell survival assay.** Adult DRG cultures from C57BL/6 and Bax<sup>-/-</sup> mice were prepared and treated with lentivirus shRNA<sup>control</sup> or shRNA<sup>mHsp25</sup> (as described above). Cells with intact neurites and round phase-bright cell bodies were counted as surviving neurons in two 25-mm<sup>2</sup> grid areas in each well. At least 500 cells were counted in each 25-mm<sup>2</sup> grid area. Baseline counts (day 0) were obtained after 2 hours in culture, and cells in the same area were counted everyday from day 1 to 9. Neurons were replaced with fresh NB medium every 3 days. Data were from 2 separate experiments repeated in triplicate.

**Western blots.** Three days after SNT, L4/L5 DRGs ipsilateral or contralateral side to the injury were pooled ( $n = 3$  per group). Uninjured ventral horns ( $n = 3$  per group) and ventral roots ( $n = 3$  per group) were dissected from hHsp27 sensory and motor lines for total hHsp27 quantification. Tissues were sonicated in lysis buffer, and protein concentration was determined. 10  $\mu$ g of protein was loaded in each lane, resolved on 4%-12% SDS poly-



acrylamide gradient gels (Invitrogen), and transferred onto a 0.2- $\mu$ m PVDF membrane (Bio-Rad). The membrane was blotted with 5% non-fat milk and incubated with anti-phospho-mHsp25-S15 (1:1,000; Stressgen), anti-phospho-mHsp25-S86 (1:1,000; Abcam), anti-phospho-hHsp27-S78 (1:1,000; Upstate), anti-phospho-hHsp27-S82 (1:1,000; Upstate), and GAPDH (1:3,000; Santa Cruz Biotechnology Inc.) overnight at 4°C, washed, and incubated with HRP-conjugated anti-rabbit or anti-mouse secondary antibodies (Pierce). Immunoreactive bands were visualized by the SuperSignal West Femto Maximum Sensitivity Substrate Kit (Pierce). Membranes were stripped and reblotted with anti-hHsp27 (1:1,000; Stressgen) or anti-mHsp25 (1:5,000; Stressgen) for total Hsp. Quantification of band intensity was performed by ImageJ software (<http://rsbweb.nih.gov/ij/>). The intensity of the total mHsp25 band was normalized to GAPDH; serine-phosphorylated forms of mHsp25/hHsp27 bands were first normalized to total mHsp25/hHsp27 and then to GAPDH. Experiments were repeated in triplicates.

**Immunohistochemistry.** hHsp27 Tg or LM mice were perfused with 4% paraformaldehyde, and L4/L5 DRGs, spinal cord, and sciatic nerve were dissected, postfixed, cryoprotected, and frozen in OCT (Tissue-Tek). Ten- $\mu$ m-thick cryosections were blocked with 0.5% bovine albumin (Sigma-Aldrich)/1% blocking reagent (Roche)/0.1% Triton X-100 in PBS and then incubated with anti-hHsp27 (1:500; Stressgen) overnight at 4°C. After 3 washes, sections were incubated with Alexa Fluor 488 anti-rabbit (1:500; Molecular Probe). Ten- $\mu$ m-thick longitudinal and four- $\mu$ m-thick transverse sections of sciatic nerves were immunostained with anti-NF-200 (1:1,500; Millipore) for neurofilament.

**Sciatic nerve pinch test.** Three days after sciatic nerve crush, anesthesia was induced with 2.5% isoflurane, and the left sciatic nerve was exposed. Then, under light anesthesia (1% isoflurane), starting distally, a series of pinches using a fine smooth forceps was delivered to the sciatic nerve moving proximally toward the injury site. The distance (mm) was recorded from the injury site to the most distal point on the nerve in which the mouse produced a reflex withdrawal when pinched. All measurements were done blinded to genotypes. To quantify the Gap-43 (1:1,000, Chemicon) immunopositive fibers; sciatic nerves were cut longitudinally into 12- $\mu$ m serial sections. The mean number of Gap-43 immunoreactive fibers per section was determined 4.5 mm beyond the injury site in 3 to 5 sections (at least 36  $\mu$ m apart) per animal. At least 3 animals from each genotype were used to determine the mean number of fibers per section.

MK2 peptide inhibitor was dissolved in saline. Approximately 1  $\mu$ l of 10  $\mu$ M MK2 inhibitor or saline as control was injected into the distal part of the sciatic nerve using a microinjector (Narushige) before the nerve crushed. Then pinch test was performed 32 hours after sciatic nerve crush. Scoring was done blinded to the genotype.

**Axon quantification.** For the 1-week transection/resuture time point, the sciatic nerve was dissected from 5-mm proximal to the suture site to the level of the flexor retinaculum in the ankle. The nerve was divided into 5-mm segments, and the number of axons in the proximal 5-mm segment and in the distal 5-, 15-, and 20-mm segments were quantified. For the 8-week transection/resuture time point, the sciatic nerve was exposed and harvested from 5-mm proximal to the suture site to the nerve trifurcation. The number of axons 5-mm proximal and 10-mm distal to the suture site was quantified. For the distal nerve segment, the number of axons in a branch of the tibial nerve within the gastrocnemius muscle just proximal to the muscle-tendineous junction was quantified. Three random pictures were taken from each 4- $\mu$ m-thick transverse section of sciatic nerve segment immunostained with anti-NF-200. The total number of axons was quantified by using ImageJ software (<http://rsbweb.nih.gov/ij/>).

**Animal behavior.** All behavioral experiments described below were conducted in a blinded fashion in a quiet room (temperature 22°C  $\pm$  1°C) from 9 AM to 6 PM. The surgeon who performed the transection/resuture surgery and the behavioral observers were not the same person.

**Assessment of sensory recovery using a pinprick assay.** Mice (7 to 9 weeks old) were placed on wire mesh cages, habituated for 3 sessions the week before surgery (sciatic nerve crush or transection/resuture), and tested on postoperative days accordingly. After a 30-minute habituation period, an Austerlitz insect pin (size 000) (FST) was gently applied to the plantar surface of the paw without moving the paw or penetrating the skin. The most lateral part of the plantar surface of the hind paw (sensory field of the sciatic nerve) was divided into 5 areas (see Figure 5A). The pinprick was applied (twice) from the most lateral toe (area E) to the heel (area A). A response was considered positive when the animal briskly removed its paw, and the mouse was graded 1 for this area, and then tested for the next one. If none of the applications elicited a positive response, the overall grade was 0. In that case, the saphenous territory of the same paw was tested as a positive control, which always elicited a positive response. Scoring was done blinded to the genotype.

**Toe spreading motor test.** To assess motor recovery after nerve injury (sciatic nerve crush or transection/resuture), the movement of the toes was evaluated. A recent study showed that the toe spreading motor test is more sensitive than analysis of gait to detect return of motor function after sciatic nerve injury (68). Mice were gently covered with a piece of cloth and lifted by the tail, uncovering the hind paws for clear observation. Under this condition, the digits spread, maximizing the space between them (the toe spreading reflex). The reappearance of this reflex results from reinnervation of the small muscles of the foot and was scored as previously described, with modifications (69): 0, no spreading; 1, intermediate spreading with all toes; and 2, full spreading (Supplemental Figure 9B). Full spreading was defined as a complete, wide, and sustained (at least 2 seconds) spreading of the toes. Mice were scored when a full response was observed on the contralateral side to the injury. Mice were evaluated twice in each experimental session with at least a 45-minute interval. In addition, 55 days after transection/resuture of the sciatic nerve, the number of toes that the mice could actively spread (single toe score) was assessed. This parameter was graded from 0 (no active spreading of any toes) to 4 (active spreading of all toes; i.e., 4 spaces between the toes). Scoring was done blinded to the genotype.

**Scar formation analysis.** Ten- $\mu$ m-thick longitudinal section of sciatic nerve was stained with picosirius red as described previously (70, 71). Briefly, cryosections were rehydrated for 2 minutes in Milli-Q water, placed in 0.2% polyphosphomolybdate for 5 minutes, and then washed in Milli-Q water for 3 times. The sections were stained with picosirius red for 1 hour, rinsed in Milli-Q water, and followed by 0.01% hydrochloric acid for 5 minutes. Sections were rinsed again in Milli-Q water before dehydrated in graded ethanol (50%–100%) and were finally rinsed in CitriSolv (Fisher) 3 times. Sections were mounted using Eukih mounting medium (Fluka), coverslipped, and allowed to dry. Images were taken under dark-field microscopy.

**Motor neuron counts.** Serial spinal cord cross-sections were stained with cresyl violet to measure motor neuron survival over a 2-mm segment of the spinal cord centered on spinal level L4–L5. Criteria used to identify motor neuron profiles were the appearance of Nissl substance, a euchromatic nucleus, and cells with a diameter of at least 12.5  $\mu$ m, and the ventral horn was defined as the area below (i.e., ventral) a horizontal line drawn at the level of the central canal (72). Motor neurons in the ipsilateral and contralateral ventral horn were counted at 100- $\mu$ m intervals in the spinal cords of hHsp27 Tg and LM control mice 55 days after SNT/resuture. Motor neuron survival was measured as a percentage of the number of neurons in the ipsilateral spinal cord relative to the number in the contralateral ventral horn of the same section. Quantification was done blinded to the genotype.

**NMJ analysis.** Mice were perfused with 4% paraformaldehyde, and the abductor digiti minimi muscle (lateral part of plantar muscles) was dissected and weighed on day 55 after SNT/resuture, postfixed, cryopro-



tected, and frozen in OCT (Tissue-Tek). 20- $\mu$ m-thick cryosections were immunostained with anti- $\alpha$ -bungarotoxin (1:1,000; Molecular Probes) and anti-NF-200 (1:1,500; Millipore) or anti-synaptophysin (1:20; Abcam). Reinnervation was quantified using a  $\times 40$  objective for overlapping neurofilament and  $\alpha$ -bungarotoxin immunoreactivity, and 3 categories could be identified: innervated, fully innervated; intermediate, partially innervated; denervated, no innervation (see Supplemental Figure 6B). Every fourth section was analyzed, and at least 600 NMJs were counted per animal. Quantification was done blinded to genotype.

**Patient data on entrapment neuropathy.** Twenty patients who were diagnosed and operated for CuTS and who were followed up for more than 2 years were evaluated for sensory and motor functional recovery. Sensory recovery on the distal phalanx of the little finger was evaluated using Semmes Weinstein monofilament testing and 2-point discrimination test. Symptoms, such as paresthesia, numbness, weakness, and the duration from the initial symptoms to operation were also noted. For motor recovery, each patient was examined preoperatively and postoperatively for the muscle power of flexor carpi ulnaris muscle, flexor digitorum profundus muscle of the ring and little finger, abductor digiti minimi muscle, and the first interosseous dorsalis muscle [IOD(1)] using manual muscle testing. Eleven patients went under surgery with complete denervation of IOD(1) muscle. The relationship between the duration of the symptoms and the recovery of both sensory and motor function after 24 months from operation was analyzed.

One hundred and thirty-six patients operated for CTS with a follow up of at least 6 months were evaluated for functional recovery. The patients were asked whether they considered themselves cured, improved, unchanged, or worsened for their sensory recovery. For motor recovery, the abductor pollicis brevis muscle (APB) was evaluated. Thirteen patients were operated with complete denervation of the APB muscle. The duration from onset to surgery was compared between patients with or without APB recovery.

**Statistics.** Data are presented as mean  $\pm$  SEM. Student's *t* test (2 groups) and 1-way ANOVA with post-hoc Newman-Keuls test (>2 groups) were used to detect statistical differences. Animal behavior data were analyzed

by 2-way repeated measures ANOVA, with post-hoc Bonferroni analysis between groups where appropriate.

**Study approval.** The animal study was reviewed and approved by Children's Hospital Boston. The patient study was reviewed and approved by the Institutional Review Board of Hamamatsu University School of Medicine. Patients provided informed consent prior to their participation in the study.

**Acknowledgments**

We thank the NIH (to C.J. Woolf; NS038253, FBG 068678), Miriam and Sheldon G. Adelson Medical Research Foundation (to C.J. Woolf, D. Geschwind, and G. Coppola), Hong Kong Croucher Foundation Fellowship (CHEM), IRP-IFP Switzerland (to M. Costigan and G. Coppola), the MICINN/Fullbright program (to E.J. Cobos), and the Fonds de la recherche en sant e du Qu ebec (to N. Ghasemlou) for financial support. We also thank the Massachusetts General Hospital Neuroscience Center Vector Development and Production Core (NIH grant P30NS045776) for production of lentivirus vectors.

Received for publication April 27, 2011, and accepted in revised form August 16, 2011.

Address correspondence to: Clifford J. Woolf, Program in Neurobiology and F.M. Kirby Neurobiology Center, Children's Hospital Boston and Department of Neurobiology, Harvard Medical School, 300 Longwood Avenue, CLS 12258, Boston, Massachusetts 02115, USA. Phone: 617.919.2265; Fax: 617.919.2772; E-mail: clifford.woolf@childrens.harvard.edu. Or to: Chi Him Eddie Ma, Department of Biology and Chemistry, City University of Hong Kong, Tat Chee Avenue, Hong Kong. Phone: 852.3442.9328; Fax: 852.3442.0522; E-mail: eddiema@cityu.edu.hk.

Chi Him Eddie Ma's present address is: Department of Biology and Chemistry, City University of Hong Kong, Hong Kong.

1. Cafferty WB, McGee AW, Strittmatter SM. Axonal growth therapeutics: regeneration or sprouting or plasticity? *Trends Neurosci.* 2008;31(5):215-220.
2. Smith DS, Skene JH. A transcription-dependent switch controls competence of adult neurons for distinct modes of axon growth. *J Neurosci.* 1997; 17(2):646-658.
3. Goldberg JL, Klassen MP, Hua Y, Barres BA. Amacrine-signaled loss of intrinsic axon growth ability by retinal ganglion cells. *Science.* 2002; 296(5574):1860-1864.
4. Chen ZL, Yu WM, Strickland S. Peripheral regeneration. *Annu Rev Neurosci.* 2007;30:209-233.
5. Terzis JK, Kokkalis ZT. Selective contralateral c7 transfer in posttraumatic brachial plexus injuries: a report of 56 cases. *Plast Reconstr Surg.* 2009;123(3):927-938.
6. Songcharoen P, Wongtrakul S, Mahaisavariya B, Spinner RJ. Hemi-contralateral C7 transfer to median nerve in the treatment of root avulsion brachial plexus injury. *J Hand Surg Am.* 2001;26(6):1058-1064.
7. Lundborg G. A 25-year perspective of peripheral nerve surgery: evolving neuroscientific concepts and clinical significance. *J Hand Surg Am.* 2000;25(3):391-414.
8. Gordon T, Tyreman N, Raji MA. The basis for diminished functional recovery after delayed peripheral nerve repair. *J Neurosci.* 2011;31(14):5325-5334.
9. Hoke A, Gordon T, Zochodne DW, Sulaiman OA. A decline in glial cell-line-derived neurotrophic factor expression is associated with impaired regeneration after long-term Schwann cell denervation. *Exp Neurol.* 2002;173(1):77-85.
10. Neumann S, Woolf CJ. Regeneration of dorsal column fibers into and beyond the lesion site following adult spinal cord injury. *Neuron.* 1999;23(1):83-91.
11. Costigan M, et al. Replicate high-density rat genome oligonucleotide microarrays reveal hundreds of regulated genes in the dorsal root ganglion after peripheral nerve injury. *BMC Neurosci.* 2002;3:16.
12. Mills CD, Bitler JL, Woolf CJ. Role of the peripheral benzodiazepine receptor in sensory neuron regeneration. *Mol Cell Neurosci.* 2005;30(2):228-237.
13. Seiffers R, Mills CD, Woolf CJ. ATF3 increases the intrinsic growth state of DRG neurons to enhance peripheral nerve regeneration. *J Neurosci.* 2007;27(30):7911-7920.
14. Costigan M, et al. Heat shock protein 27: developmental regulation and expression after peripheral nerve injury. *J Neurosci.* 1998;18(15):5891-5900.
15. Nakagomi S, Suzuki Y, Namikawa K, Kiryu-Seo S, Kiyama H. Expression of the activating transcription factor 3 prevents c-Jun N-terminal kinase-induced neuronal death by promoting heat shock protein 27 expression and Akt activation. *J Neurosci.* 2003; 23(12):5187-5196.
16. Benn SC, et al. Hsp27 upregulation and phosphorylation is required for injured sensory and motor neuron survival. *Neuron.* 2002;36(1):45-56.
17. Evgrafov OV, et al. Mutant small heat-shock protein 27 causes axonal Charcot-Marie-Tooth disease and distal hereditary motor neuropathy. *Nat Genet.* 2004;36(6):602-606.
18. Williams KL, Mearow KM. Phosphorylation status of heat shock protein 27 influences neurite growth in adult dorsal root ganglion sensory neurons in vitro. *J Neurosci Res.* 2011;89(8):1160-1172.
19. During RL, et al. Anthrax lethal toxin paralyzes actin-based motility by blocking Hsp27 phosphorylation. *EMBO J.* 2007;26(9):2240-2250.
20. Pichon S, Bryckaert M, Berrou E. Control of actin dynamics by p38 MAP kinase - Hsp27 distribution in the lamellipodium of smooth muscle cells. *J Cell Sci.* 2004;117(pt 12):2569-2577.
21. Banzai Y, Miki H, Yamaguchi H, Takenawa T. Essential role of neural Wiskott-Aldrich syndrome protein in neurite extension in PC12 cells and rat hippocampal primary culture cells. *J Biol Chem.* 2000;275(16):11987-11992.
22. Chaudhuri S, Smith PG. Cyclic strain-induced HSP27 phosphorylation modulates actin filaments in airway smooth muscle cells. *Am J Respir Cell Mol Biol.* 2008;39(3):270-278.
23. Chen HF, Xie LD, Xu CS. Role of heat shock protein 27 phosphorylation in migration of vascular smooth muscle cells. *Mol Cell Biochem.* 2009;327(1-2):1-6.
24. Gupton SL, Gertler FB. Filopodia: the fingers that do the walking. *Sci STKE.* 2007;2007(400):re5.
25. Oldham MC, et al. Functional organization of the transcriptome in human brain. *Nat Neurosci.* 2008;11(11):1271-1282.
26. Griffin RS, et al. Complement induction in spinal cord microglia results in anaphylatoxin C5a-mediated pain hypersensitivity. *J Neurosci.* 2007; 27(32):8699-8708.
27. Costigan M, Scholz J, Woolf CJ. Neuropathic pain: a maladaptive response of the nervous system to damage. *Annu Rev Neurosci.* 2009;32:1-32.
28. Costigan M, et al. Multiple chronic pain states are associated with a common amino acid-changing



- allele in KCNS1. *Brain*. 2010;133(9):2519–2527.
29. Mallavarapu A, Mitchison T. Regulated actin cytoskeleton assembly at filopodium tips controls their extension and retraction. *J Cell Biol*. 1999;146(5):1097–1106.
30. Markus A, Zhong J, Snider WD. Raf and akt mediate distinct aspects of sensory axon growth. *Neuron*. 2002;35(1):65–76.
31. Stokoe D, Engel K, Campbell DG, Cohen P, Gaestel M. Identification of MAPKAP kinase 2 as a major enzyme responsible for the phosphorylation of the small mammalian heat shock proteins. *FEBS Lett*. 1992;313(3):307–313.
32. Willis D, et al. Differential transport and local translation of cytoskeletal, injury-response, and neurodegeneration protein mRNAs in axons. *J Neurosci*. 2005;25(4):778–791.
33. Toth CC, et al. Locally synthesized calcitonin gene-related peptide has a critical role in peripheral nerve regeneration. *J Neuropathol Exp Neurol*. 2009;68(3):326–337.
34. Willis DE, et al. Extracellular stimuli specifically regulate localized levels of individual neuronal mRNAs. *J Cell Biol*. 2007;178(6):965–980.
35. Hoke A, et al. Schwann cells express motor and sensory phenotypes that regulate axon regeneration. *J Neurosci*. 2006;26(38):9646–9655.
36. Richardson PM, Verge VM. The induction of a regenerative propensity in sensory neurons following peripheral axonal injury. *J Neurocytol*. 1986;15(5):585–594.
37. Lavoie JN, Gingras-Breton G, Tanguay RM, Landry J. Induction of Chinese hamster HSP27 gene expression in mouse cells confers resistance to heat shock. HSP27 stabilization of the microfilament organization. *J Biol Chem*. 1993;268(5):3420–3429.
38. Garrido C, Bruey JM, Fromentin A, Hammann A, Arrigo AP, Solary E. HSP27 inhibits cytochrome c-dependent activation of procaspase-9. *FASEB J*. 1999;13(14):2061–2070.
39. Jankowski MP, Cornuet PK, McIlwrath S, Koerber HR, Albers KM. SRY-box containing gene 11 (Sox11) transcription factor is required for neuron survival and neurite growth. *NeuroScience*. 2006;143(2):501–514.
40. Raivich G, et al. The AP-1 transcription factor c-Jun is required for efficient axonal regeneration. *Neuron*. 2004;43(1):57–67.
41. Sheu JY, Kulhanek DJ, Eckenstein FP. Differential patterns of ERK and STAT3 phosphorylation after sciatic nerve transection in the rat. *Exp Neurol*. 2000;166(2):392–402.
42. Jenkins R, McMahon SB, Bond AB, Hunt SP. Expression of c-Jun as a response to dorsal root and peripheral nerve section in damaged and adjacent intact primary sensory neurons in the rat. *Eur J Neurosci*. 1993;5(6):751–759.
43. Richardson PM, Issa VM. Peripheral injury enhances central regeneration of primary sensory neurons. *Nature*. 1984;309(5971):791–793.
44. Vaudano E, Campbell G, Hunt SP, Lieberman AR. Axonal injury and peripheral nerve grafting in the thalamus and cerebellum of the adult rat: upregulation of c-jun and correlation with regenerative potential. *Eur J Neurosci*. 1998;10(8):2644–2656.
45. Fu SY, Gordon T. Contributing factors to poor functional recovery after delayed nerve repair: prolonged axotomy. *J Neurosci*. 1995;15(5 pt 2):3876–3885.
46. Fu SY, Gordon T. Contributing factors to poor functional recovery after delayed nerve repair: prolonged denervation. *J Neurosci*. 1995;15(5 pt 2):3886–3895.
47. Sulaiman OA, Gordon T. Effects of short- and long-term Schwann cell denervation on peripheral nerve regeneration, myelination, and size. *Glia*. 2000;32(3):234–246.
48. Buchthal F, Kuhl V. Nerve conduction, tactile sensibility, and the electromyogram after suture or compression of peripheral nerve: a longitudinal study in man. *J Neurol Neurosurg Psychiatry*. 1979;42(5):436–451.
49. Nagano A, Tsuyama N, Ochiai N, Hara T, Takahashi M. Direct nerve crossing with the intercostal nerve to treat avulsion injuries of the brachial plexus. *J Hand Surg Am*. 1989;14(6):980–985.
50. Giuffrè JL, Kakar S, Bishop AT, Spinner RJ, Shin AY. Current concepts of the treatment of adult brachial plexus injuries. *J Hand Surg Am*. 2010;35(4):678–688.
51. Saito H, Dahlin LB. Expression of ATF3 and axonal outgrowth are impaired after delayed nerve repair. *BMC Neurosci*. 2008;9:88.
52. Terenghi G. Peripheral nerve regeneration and neurotrophic factors. *J Anat*. 1999;194(pt 1):1–14.
53. Gallo G. RhoA-kinase coordinates F-actin organization and myosin II activity during semaphorin-3A-induced axon retraction. *J Cell Sci*. 2006;119(pt 16):3413–3423.
54. Gallo G. Myosin II activity is required for severing-induced axon retraction in vitro. *Exp Neurol*. 2004;189(1):112–121.
55. Luo L, O'Leary DD. Axon retraction and degeneration in development and disease. *Annu Rev Neurosci*. 2005;28:127–156.
56. Reynolds ML, Woolf CJ. Terminal Schwann cells elaborate extensive processes following denervation of the motor endplate. *J Neurocytol*. 1992;21(1):50–66.
57. Magill CK, et al. Reinnervation of the tibialis anterior following sciatic nerve crush injury: a confocal microscopic study in transgenic mice. *Exp Neurol*. 2007;207(1):64–74.
58. Son YJ, Thompson WJ. Nerve sprouting in muscle is induced and guided by processes extended by Schwann cells. *Neuron*. 1995;14(1):133–141.
59. O'Malley JP, Waran MT, Balice-Gordon RJ. In vivo observations of terminal Schwann cells at normal, denervated, and reinnervated mouse neuromuscular junctions. *J Neurobiol*. 1999;38(2):270–286.
60. Yang JF, Cao G, Koirala S, Reddy LV, Ko CP. Schwann cells express active agrin and enhance aggregation of acetylcholine receptors on muscle fibers. *J Neurosci*. 2001;21(24):9572–9584.
61. De Winter F, et al. The expression of the chemorepellent Semaphorin 3A is selectively induced in terminal Schwann cells of a subset of neuromuscular synapses that display limited anatomical plasticity and enhanced vulnerability in motor neuron disease. *Mol Cell Neurosci*. 2006;32(1–2):102–117.
62. Sanes JR, Schachner M, Covault J. Expression of several adhesive macromolecules (N-CAM, L1, J1, NILE, uvomorulin, laminin, fibronectin, and a heparan sulfate proteoglycan) in embryonic, adult, and denervated adult skeletal muscle. *J Cell Biol*. 1986;102(2):420–431.
63. Wu H, Xiong WC, Mei L. To build a synapse: signaling pathways in neuromuscular junction assembly. *Development*. 2010;137(7):1017–1033.
64. Oldham MC, Horvath S, Geschwind DH. Conservation and evolution of gene coexpression networks in human and chimpanzee brains. *Proc Natl Acad Sci U S A*. 2006;103(47):17973–17978.
65. Sena-Esteves M, Tebbets JC, Steffens S, Crombleholme T, Flake AW. Optimized large-scale production of high titer lentivirus vector pseudotypes. *J Virol Methods*. 2004;122(2):131–139.
66. Knudson CM, Tung KS, Tourtellotte WG, Brown GA, Korsmeyer SJ. Bax-deficient mice with lymphoid hyperplasia and male germ cell death. *Science*. 1995;270(5233):96–99.
67. Caroni P. Overexpression of growth-associated proteins in the neurons of adult transgenic mice. *J Neurosci Methods*. 1997;71(1):3–9.
68. Bozkurt A, et al. Aspects of static and dynamic motor function in peripheral nerve regeneration: SSI and CatWalk gait analysis. *Behav Brain Res*. 2011;219(1):55–62.
69. Azzouz M, Kenel PF, Warter JM, Poindron P, Borg J. Enhancement of mouse sciatic nerve regeneration by the long chain fatty alcohol, N-Hexacosanol. *Exp Neurol*. 1996;138(2):189–197.
70. Junqueira LC, Bignolas G, Brentani RR. Picrosirius staining plus polarization microscopy, a specific method for collagen detection in tissue sections. *Histochem J*. 1979;11(4):447–455.
71. Atkins S, et al. Interleukin-10 reduces scarring and enhances regeneration at a site of sciatic nerve repair. *J Peripher Nerv Syst*. 2007;12(4):269–276.
72. Ghasemlou N, et al. Mitogen-activated protein kinase-activated protein kinase 2 (MK2) contributes to secondary damage after spinal cord injury. *J Neurosci*. 2010;30(41):13750–13759.